Review

Porous Graphitic Carbon Nitride-Based Photocatalysts for Antibiotic Degradation

Zhaoqiang Wang [1], Guixiang Ding [1], Juntao Zhang [1], Peng Wang [2], Qi Lv [3], Yonghao Ni [4] and Guangfu Liao [1,*]

[1] National Forestry and Grassland Administration Key Laboratory of Plant Fiber Functional Materials, College of Materials Engineering, Fujian Agriculture and Forestry University, Fuzhou 350002, China
[2] Shandong Chambroad Petrochemicals Co., Ltd., Binzhou 256500, China
[3] PCFM Lab, GD HPPC Lab, School of Materials Science and Engineering, Sun Yat-sen University, Guangzhou 510275, China
[4] Department of Chemical Engineering, University of New Brunswick, Fredericton, NB E3B 5A3, Canada
* Correspondence: liaogf@mail2.sysu.edu.cn
Received: 29 November 2023; Revised: 18 January 2024; Accepted: 24 January 2024; Published: 5 March 2024

Abstract: Photocatalytic technology is a promising strategy for solving antibiotic pollution present in the water system. Porous carbon nitride (PCN) material has been considered as a potential candidate to solve the above problem due to the abundant reaction sites, large specific surface area and narrow band gap. Recently, substantial research focus on promoting photocatalytic activity of PCN-based material via improving photogenerated carrier separation and band gap structure has been completed. However, only a few works summarize and discuss the results of research on photocatalytic antibiotic degradation by PCN-based photocatalysts in recent years. Thus, a review on recent developments in PCN-based photocatalysts research is urgently needed to further promote its advancement. In this review, the synthesis strategies, structure design and photocatalytic application of antibiotic degradation over PCN-based photocatalysts are listed in detail. Finally, a brief conclusion has been discussed deeply, which focuses on the future challenges and expectations of PCN-based photocatalysts for photocatalytic antibiotic degradation. This review offers a novel viewpoint on the use of PCN-based material in photocatalytic antibiotic degradation and highlights its significant potential as a photocatalyst. In short, the application of PCN-based materials in the photocatalytic degradation of antibiotics is very promising, according to objective assessments.

Keywords: porous carbon nitride; photocatalysts; antibiotic degradation

1. Introduction

The discovery of antibiotics has significantly advanced human medicine by effectively neutralizing pathogenic microorganisms [1–4]. This has proved to be a powerful tool in the medical field, as antibiotics have provided a way to combat various infectious diseases [5–7]. Unfortunately, people have become reliant on antibiotics, leading to their excessive use [8–10]. Overuse of antibiotics has resulted in their incomplete metabolism in the human and animal body. Consequently, they are partially excreted via urine and feces, leading to the abundant presence of antibiotics in domestic sewage, groundwater, and surface water. Although antibiotics show a shorter half-life compared to other organic materials, their long-term presence in the environment will cause the evolution of antibiotic-resistant genes and drug-resistant bacteria, accelerating the spread of resistance, which will pose a serious threat to the ecology and human living environment in the long-term [11]. Therefore, it is essential to develop effective technologies to remove antibiotics completely from water.

In recent years, several options have been employed to combat antibiotic pollution, such as flocculation, membrane separation, adsorption, and biodegradation [12]. Nevertheless, the practical application of these methods has been restricted due to their high cost, poor stability and low recyclability [5]. Thus, developing new techniques to manage antibiotic contamination in both environmental and chemical domains continues to pose a challenge [13–15]. In contrast, the photocatalytic approach represents a cost-effective and environmentally-friendly solution that employs sunlight to degrade antibiotics [16]. When light irradiates the semiconductor, it generates reducing photogenerated electrons (e^-) and oxidizing photogenerated holes (h^+) that migrate to the semiconductor surface. Some of the generated e^- convert absorbed oxygen into superoxide radicals ($\bullet O_2^-$), while

some of the generated h^+ combine with water and antibiotics to produce hydroxyl radicals (•OH) and degrade the antibiotics [17]. Herein, efficient carrier separation, light harvesting, and redox intensity are crucial factors in determining the catalytic activity of semiconductors. Rational structural design and material selection can enhance the photocatalytic antibiotics degradation.

Carbon nitride (g-C_3N_4) material is a non-metallic covalent polymer with a narrow band gap, outstanding chemical stability, and is non-toxic and non-polluting [16,18–20]. Therefore, it is deemed a promising candidate for photocatalysis. However, conventional g-C_3N_4 materials are synthesized via polymerization of N-containing precursors at high temperatures, resulting in a stable block structure that limits their catalytic activity [21]. Fortunately, the nanostructure design of g-C_3N_4 has rapidly developed in recent years, especially the PCN advancement [22]. PCN can enhance the photocatalytic activity of g-C_3N_4 in many aspects, for example, the presence of a porous structure can increase the specific surface area of g-C_3N_4 and the surface-active site [21,23]. In addition, porous structure endows the narrow band gap and the rapid electron migration. At same time, in order to further improve the catalytic activity of PCN, substantial research based on PCN have been carried out.

In this review, we summarized the development, synthesis strategies, modification strategies and antibiotic degradation applications of PCN in the field of photocatalysis in recent years. Firstly, the common approaches for preparing PCN are divided in to bottom-up and top-down approach. The bottom-up mainly include template method and supramolecular assembly, and top-down approach categories chemical exfoliation and thermal oxidation. Then, the morphological structure and functional modification are also separately introduced in detail. The photocatalytic mechanisms of PCN with different morphologies and the corresponding photocatalytic functional properties are also described. Subsequently, the applications of PCN-based photocatalysts in photocatalytic antibiotic degradation, for instance, tetracycline degradation, ciprofloxacin degradation, norfloxacin degradation et al. are summarized. Finally, a brief summary and perspectives on the challenges and future research topics of PCN-based photocatalysts in photocatalytic antibiotic degradation are discussed.

2. Synthesis Strategies

2.1. Bottom-up Approaches

The bottom-up approaches play a key role in preparing PCN, which is attributed to the strategy directly obtains PCN from N-containing precursor. According to the previous reported, bottom-up methods greatly protect the structure of the g-C_3N_4, avoid the useless defects and promote the separation of photogenerated carriers [24,25]. The bottom-up approaches applied in preparing PCN are generally divided into two methods: (1) The templating method adapt physical pathway to form porous structure; (2) Heteroatom-mediated method, the porous formation of PCN is constructed via the van der Waals weak interaction between molecular [26].

2.1.1. Template Method

For a long time, template-assisted method has been considered as a mainstream to tune the microscopic size, pore structure and micro-morphology of PCN [27]. Mesoporous g-C_3N_4 possesses unique surface characteristics and physicochemical properties. A valid template ought to have the following distinguishing features. (i) Excellent structure for synthesis of PCN e.g., opened crystalline pore wall and large specific surface area. (ii) No side reactions will occur between template and sample. (iii) Templates are easy to remove. The template methods are mainly divided into hard template method and soft template method. Figure 1 shows a simple schematic of the preparation processes of these two approaches.

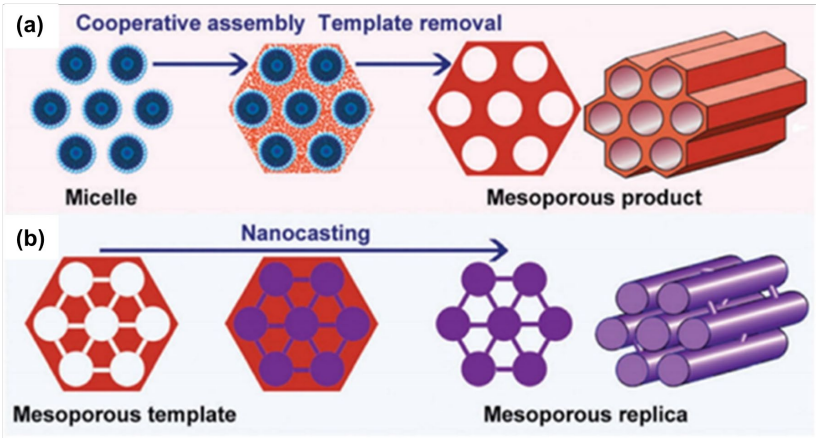

Figure 1. (**a**) Soft and (**b**) hard template methods for preparation of g-C_3N_4 mesoporous nanotubes. Figures taken with permission from reference [28].

(1) Hard Template Methods

Hard template method also known as nanocasting methods refers to the use of solid materials such as silica, alumina oxide or carbon to "cast" a second material which can controlling grain size and surface area [29]. Recently, more and more researchers are committed to using hard template to fabricate PCN. Groenewolt and coworkers [30] used the template method for the first time to prepare PCN. Cyanamide (CH_2N_2) and monolithic silicon dioxide were used as a molecular precursor and the hard template to synthesis PCN with excellent result. The preparation of the hard template is divided into three steps: Firstly, preparing the hard templates which facilitate the formation of porous structures. Secondary, coating the precursor to fill the template. Finally, eliminating the hard template and exposing the finished product. However, the above approach is still flawed, which is mainly attributed to several reasons as follow: (i) Templates with a small size are difficult to synthesize. And after completion of the reaction, there remains a residue of the initial template. (ii) Hard template surface properties will damage the coating process even influence the performance of the product. (iii) Coating is a self-assembly process and does not guarantee uniform coverage of the target material over the hard template. This may result in morphological and structural differences. (iv) The strong acids and bases used to remove templates, such as NaOH, HF, and NH_4HF_2 solution, which is unfriendly for environment, safe operation and even the formation of the target material [31–33].

According to the synthesis pathway, the hard template methods can be divided into two types: (i) Precursor coating method, the pore structure similar to template is constructed through covering the precursor on the surface of hard template. (ii) Hard template coating method, the pore materials of similar size to template are synthesized via coating the hard template on the surface of precursor. Another way to categorize them is in terms of template reservations: Remove template involves template deletion at the end of reaction. The removal templates generally include silica, alumina oxide, carbon nanofibers (N-CNFs) and calcium salts nano-particles [34–36]. For example, Tian et al. [37] successfully synthesized PCN with alveolate structure by using SiO_2 microspheres and dicyandiamide (DCDA) as the hard template and precursor. The homogenous solution of colloidal silica and DCDA played the important roles in the synthesis of PCN. Figure 2a shows processes of typical preparation of hard template, the DCDA uniformly coated by SiO_2 microspheres was prepared by the order of ultrasonic treatment, calcination and washed with deionized water. Finally, PCN was obtained after SiO_2 microspheres are removed with 20 wt% HF. The alveolar skeleton structure of ACN obtained after the removal of SiO_2 nanospheres is shown in Figure 2b–d revealed the ordered alveolar structure of the composite. According to EDS diagrams (Figure 2e–f), the distribution of elements C, N and Co, indicating that Co has been successfully loaded and uniformly dispersed on the composite. The specific surface area (SBET) of PCN was up to 18.19 $m^2\ g^{-1}$ and the average pore size was about 39.91 nm, which means the prepared PCN had better photocatalytic performance than spring g-C_3N_4 due to the porous structure is benefit to the exposing of active sites, light-harvesting and photogenerated carrier migration.

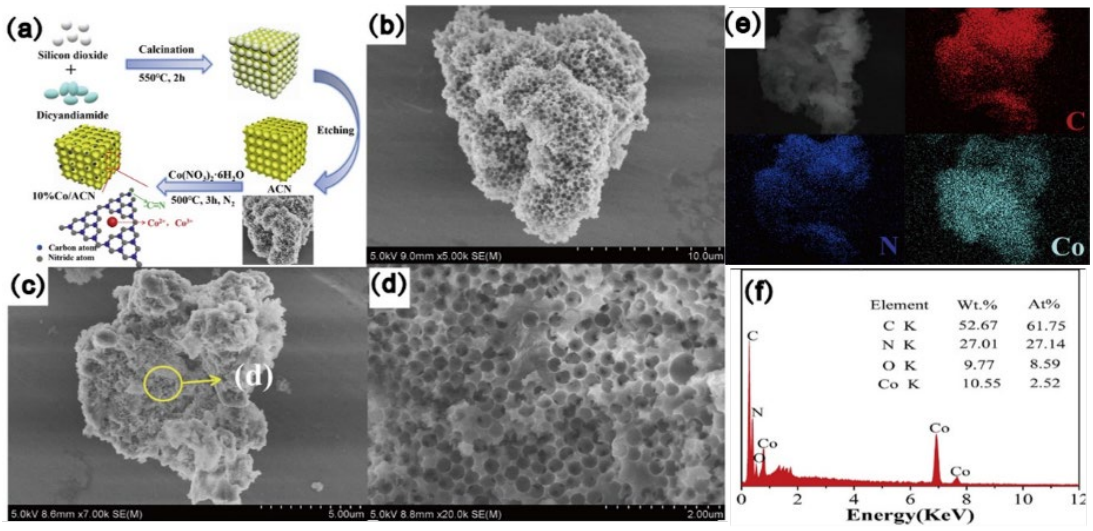

Figure 2. (**a**) Schematic illustration of the formation process of 10% Co/ACN hybrid photocatalysts; (**b**) TEM images of CAN; (**c,d**) 10%Co/CAN; (**e**) Elemental mapping images of 10%Co/ACN, EDS spectrum of (**f**). Figures taken with permission from reference [37].

Retain the template method. The precursor covers the surface of a porous material, which is used as a self-template to form a heterogeneous structure that contacts the interface. As a result, the photocatalytic activity of the prepared samples is improved. Ma et al. [38] successfully prepared PCN using titanium dioxide (TiO_2) hollow microspheres. The production method is shown in Figure 3a. Titanium dioxide hollow microspheres were fabricated using a simple hydrothermal method with glucose as a template. Pure g-C_3N_4 was synthesized through heating melamine. The resulting bulk g-C_3N_4 was ground into a fine powder and then sliced thinly using ultrasound to achieve a uniform g-C_3N_4 suspension. To create porous structures, the suspension was used to disperse titanium dioxide hollow microspheres through bath evaporation and drying. The core-shell TiO_2@g-C_3N_4 structure seen in CNT-15 (Figure 3b) exhibits TiO_2 hollow microspheres at its core and g-C_3N_4 as its shell. TEM characterization (Figure 3c) confirmed the coating of g-C_3N_4 on the surface of TiO_2 hollow microspheres. The close proximity of the TiO_2 microspheres and g-C_3N_4 facilitated the transfer of photogenerated electrons at the interface between g-C_3N_4 and TiO_2, leading to an enhancement in photocatalytic activity.

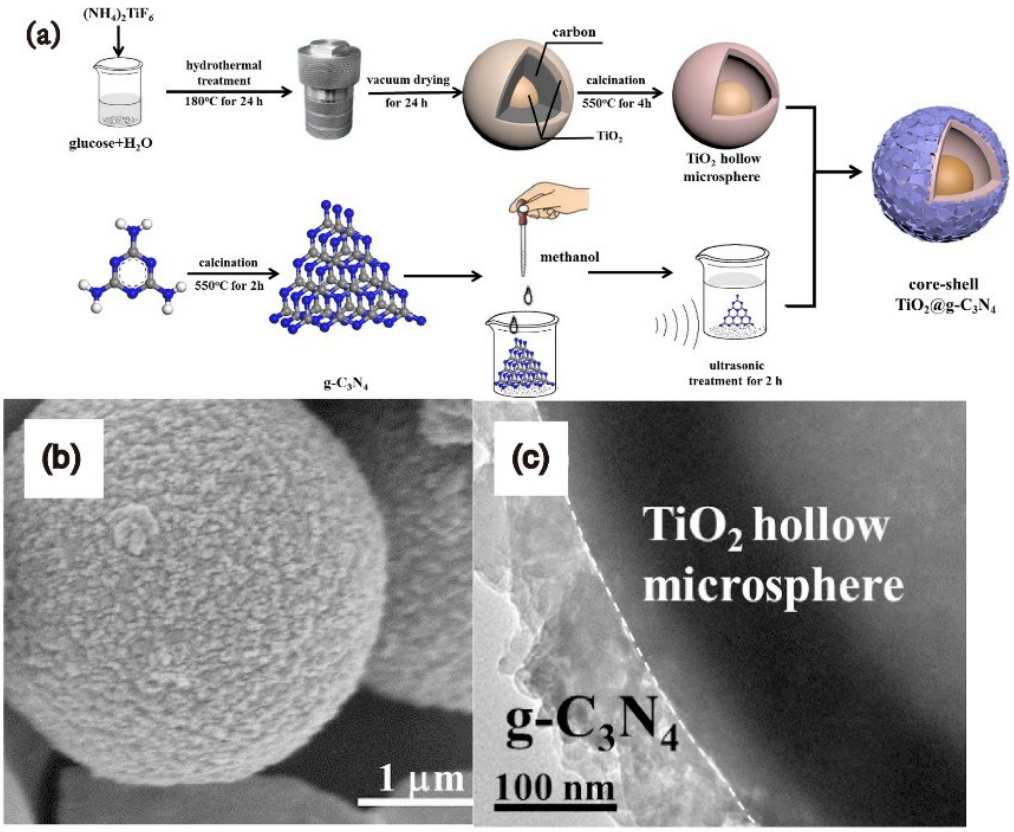

Figure 3. (**a**) Schematic illustration for the preparation of CNT-x composites; (**b**) SEM images of CNT-15 TEM; (**c**) images of CNT-15. Figures taken with permission from reference [38].

The retention hard-template methodology is convenient and eco-friendly than alternative hard-template techniques. Nonetheless, the prerequisites for self-templating embody: (i) the prescribed hard template substrate ought to exhibit a porous constitution; and (ii) the material must be thermally stable and preserve its porous configuration for at least the precursor deposition stage. Infrequent reports have been documented due to the demanding template requisites. The stencil coating method is another hard stencil technique. Its fundamental principle is to place the template on top of the precursor material, then eliminate the template to achieve a porous coordination network closely resembling the template's particle size. For example, Chen et al. [39] successfully synthesized PCN using commercial calcium carbonate particles as a hard template. The brief operation is to add a certain amount of calcium carbonate nanoparticles into dicyandiamide solution, disperse treatment, after 520 degrees of calcination and finally remove calcium carbonate particles with hydrochloric acid solution. This method is more environmentally friendly than conventional methods because calcium carbonate is easier to remove with a dilute hydrochloric acid solution. And the low-cost solution is obtained, which provides a reliable way for

industrial preparation. Hard template has great potential in increasing specific surface area, reducing carrier recombination rate and enhancing visible light absorption. However, Toxic removal agent and complex synthetic pathways limit the use of templates. Therefore, it is one of the key problems to further explore the high-performance template, optimize the synthesis path, and adopt the self-template or even no template method to prepare PCN by hard template method.

(2) Soft Template Methods

In the development process of hard templating, soft templating has gained considerable attention for its uncomplicated preparation and lack of template requirements. The soft templating route not only simplifies the overall synthesis process, but also allows for the adjustment of form through selection of various soft templates. Soft template structure guides, comprising of amphiphilic block polymers, surfactants, or bubble methods, can be utilized for the construction of nanostructured g-C_3N_4 [40]. The amphiphilic block polymer method is excessively complex to execute and rarely documented. Conversely, the surfactant and bubble techniques are more frequently utilized. The production of bubble template is the crucial factor in synthesizing PCN using the bubble method. These methods automatically eliminate the soft template throughout the reaction process. Therefore, diverse soft templates and precursors can be utilized to reasonably design and prepare PCN. The production of bubble template is the crucial factor in synthesizing PCN using the bubble method. In summary, the gas released by the soft template during the precursor calcination process optimizes the transfer of reaction heat at high temperatures and acts as a template to promote the formation of porous structures. For instance, Liu et al. [41] successfully synthesized porous g-C_3N_4 by a simple co-pyrolysis method using melamine and NH_4HCO_3 as co-precursors. NH_4HCO_3 was also used as a soft bubble template. As shown in Figure 4a, a certain mass ratio of melamine was fully mixed with NH_4HCO_3 to form a mixture. The mixture was then calcined in a Muffle furnace. NH_4HCO_3 decomposes and provides a dynamic gas template to forms a porous structure on the g-C_3N_4 sheet. The photocatalytic mechanism is shown in Figure 4b. A red shift at 807 and 1568 cm^{-1} was shown in FTIR (Figure 4c), which indicated a lamellar structure. From the band structure diagram (Figure 4d) can be found that CB energy level increases significantly, which is conducive to the generation of more electrons with strong reducing power or superoxide free radicals ($\bullet O^{2-}$) with strong oxidizing power, promoting photocatalytic activity. The surface area of the prepared PCN was 7.692 m^2 g^{-1}, which was more than twice that of g-C_3N_4 (3.043 m^2 g^{-1}). However, although the soft template method is easy to operate and low cost, it will release much toxic and harmful gases in the process of use, which will cause harm to the environment. Thus, how to develop environmentally friendly, green and pollution-free template is the focus of the future work.

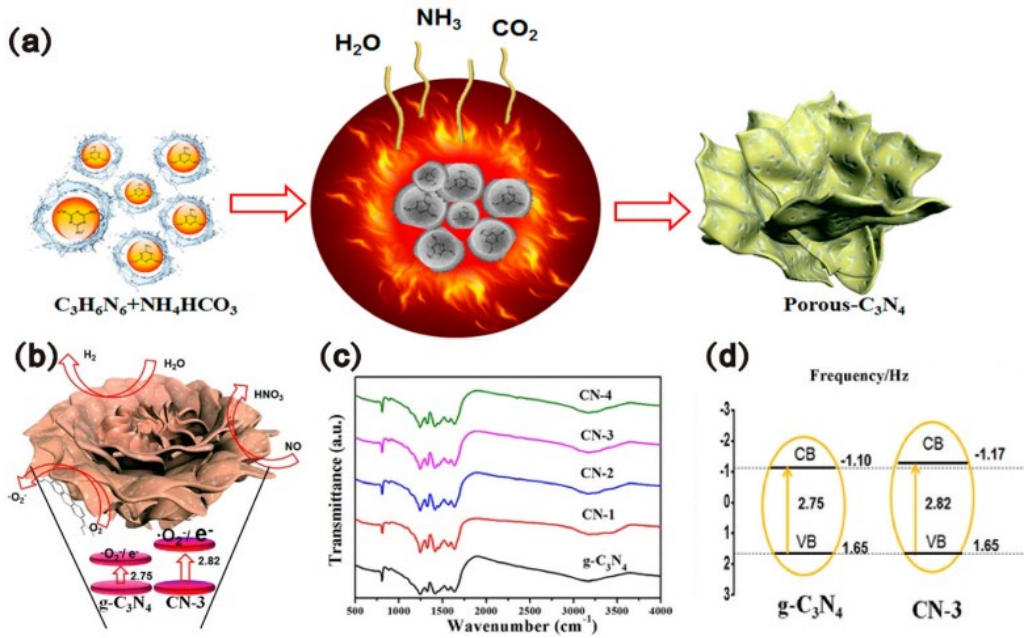

Figure 4. (**a**) hematic illustration of the preparation of the modified g-C_3N_4 samples; (**b**) Schematic diagrams of the photocatalytic mechanism of g-C_3N_4 and CN-3 under visible light irradiation; (**c**) FTIR spectra of bulk g-C_3N_4 and CN-X (X = 1, 2, 3, 4); (**d**) Schematic illustration of the energy band structures of pure g-C_3N_4 and CN-3. Figures taken with permission from reference [41].

Another soft template method is the surfactant method, which uses the template as a surface agent mixed with a precursor to synthesize PCN. Wang et al. [42] first prepared PCN with different active agents and explored its application. Although the prepared samples have a large specific surface area, only a few of them have porous structures. For example, in a sample with Triton X-100 and ionic liquids added. Therefore, the choice of surfactant is very important for the formation of porous structure. Suitable surfactants need to have a certain degree of thermal and chemical stability, and easily decompose during the reaction process. Fan et al. [43]. explored the effects of different temperatures on surfactants. In the synthesis process, melamine and Triton X-100 were added to distilled water at a certain mass ratio and then heated in an oil bath to obtain melamine sulfate (MAS). Then, different PCN samples were obtained by calcination of MST at different temperatures. The results show that the higher the temperature, the larger the specific surface area of the sample. However, the photocatalytic performance of the sample did not increase with the increase of surface area due to band gap. Therefore, balancing the relationship between surface area and band gap is a key to the use of surface activity. Compared with the hard template, the soft template is simple to synthesize, convenient to operate, low cost, and has a broad prospect of exploration. However, the soft template cannot strictly control the pores of the porous products, and the reaction process may have side reactions with the precursor, resulting in decreased photocatalytic activity. Therefore, it is still a challenge to explore the soft template synthesis of green high-performance PCN.

2.1.2. Supramolecular Assembly

In recent years, researchers have proposed the concept of molecular self-assembly due to the complex synthesis pathway, the generation of side reactions and the use of toxic removers. Compared with template method, molecular self-assembly method is easier to control sample morphology through hydrogen bonding. Supramolecular assembly is the spontaneous association of nitrogen-rich precursors (such as melamine, cyanamide, cyanuric acid, etc.) into stable aggregates under equilibrium conditions through non-covalent interactions to form definite composition and structure (Figure 5) [44]. Hydrogen bond plays a key role in the process of molecular self-assembly due to its reversibility. During calcination, hydrogen bonds are released to create a very high degree of freedom and form a porous structure.

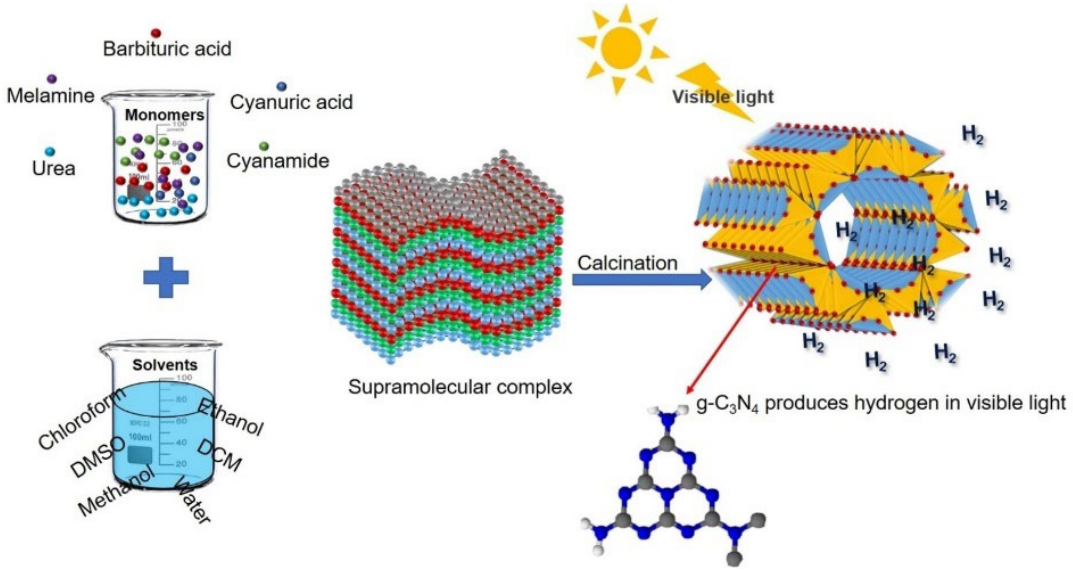

Figure 5. Schematic representation of supramolecular assembles tailored g-C_3N_4 for hydrogen generation under visible light. Figures taken with permission from reference [44].

Cyanuric acid-melamine complex (CM) is a famous supramolecular polymer. The presence of three hydrogen bonds in the CM allows it to adapt to a variety of forms, resulting in different structures in various solvents, such as linear, fold or rosette bands [45]. Recently Shalom et al. [46] used supramolecular self-assembly method to obtain different forms of PCN through different condensation time. The results show that the longer the calcination time, the smaller the sample size and pore size. This is due to the specific growth of CM under the action of ethanol and hydrogen bond. The morphology, structure and pore size of PCN are affected by different treatment of molecular aggregates. For example, Zhou et al. [47] Successfully through the impassable heat treatment of the supramolecular precursor of melamine formed in water as a solvent to controlled the dimensions and morphology of PCN (Figure 6a). Through different heat treatment, the three-dimensional (3D) hexagonal prism precursor can

be transformed into 3D g-C_3N_4 loofah structure and ultra-thin 2D (Figure 6b). The dimensional and morphological modulation strategies proposed in this scheme are expected to broaden our horizons.

So far, hydrogen bonding based on strong intermolecular directivity and saturation has been successfully applied to the formation of hollow supramolecular structures [37]. The formation of supramolecules plays an important role in the regulation of g-C3N4 band structure [38]. Molecular self-assembly in aqueous solvent is easy to form stable, large size of hydrogen containing supramolecular premise. However, many supramolecular premises can only self-assemble in organic solvents at room temperature, such as CM [39]. Finally, although solvents can influence the dynamic and equilibrium geometric behavior of monomers, they do not provide a uniform chemical environment to facilitate molecular self-assembly [40]. Studies have shown that benzene substituted melamine can also affect the morphology, chemistry and crystal structure of g-C_3N_4 material [41]. But their toxicity limits their use. Therefore, the supramolecular self-assembly method for the synthesis of green, high-performance PCN is still a challenge.

The template method or self-assembly method based on intermolecular forces can be used in the bottom-up approach to form ultra-thin nanosheets with large transverse size and controlled thickness in fewer steps and less time. The use of a suitable template can provide a platform for the preparation of PCN nanosheets by the precursor system.

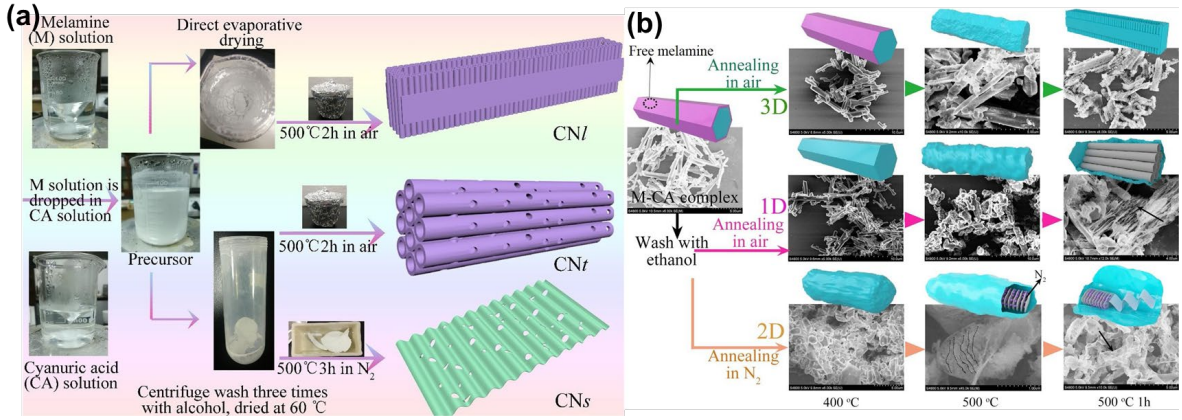

Figure 6. (**a**) Fabrication process of CNl, CNt and CNs; (**b**) The evolution process and conjectural mechanism of M-CA complex in the process of heating. The first, second, and third lines are the SEM images and speculative models of 3D CNl, 1D CNt and 2D CNs at different temperatures, respectively. Figures taken with permission from reference [47].

2.2. Top-down Approaches

The top-down methodology achieves small PCN particles from large and thick nano-g-C_3N_4 through various driving forces. A reasonable top-down synthesis strategy can break the strong hydrogen bonding and van der Waals accumulation in g-C_3N_4, and improve the specific surface area and dispersion of g-C_3N_4 in the reaction medium [48–50]. The top-down method mainly includes thermal oxidation, chemical peeling, ultrasonic separation, ball milling and other methods to convert BCN into PCN. In this section, we will describe the application of these methods to the production of PCN.

2.2.1. Chemical Exfoliation

The high degree condensation of the tri-s-triazine nuclei results in increased van der Waals interactions between carbon nitride layers, providing high thermal resistance similar to that of graphene. The tough exfoliation of g-C_3N_4 into single or few-layered nanosheets remains a grand challenge for the fundamental studies and applications of PCN. Based on the fact that the interlayer van der Waals force of g-C_3N_4 is weak, PCN nanosheets can be synthesised by chemical exfoliation. Liu et al. [51] have developed a simple two-step method for producing few-layered PCN. The research shows that rapid thermal etching and gas stripping can weaken the van der Waals forces between carbon nitride layers. This process not only peels CN into nanosheets with a specific surface area of 70.2 $m^2\ g^{-1}$, but also effectively removes graphite carbon impurities. Numerous exfoliants, such as potent acids (e.g., H_2SO_4), ammonia (e.g., HNO_3), and other high oxides (e.g., H_2O_2, $K_2Cr_2O_7$), can be employed as chemical exfoliants for BCN [52,53]. Chemical oxidation of g-C_3N_4 with $K_2Cr_2O_7$-H_2SO_4 creates hydrophilic functional groups like COOH and –OH at the open ends or structural defects of the g-C_3N_4-body. This leads to the formation of porous aqueous dispersion g-C_3N_4. Furthermore, acid oxidation results in the creation of hydroxyl and carboxyl

groups on the surface of the base and the formation of a porous structure in g-C_3N_4. [54] Shi et al. [55] prepared PCN nanosheets by chemical stripping. As shown in the Figure 7a, the bulk carbon nitride (BCN) is first heated and protonated with the phosphoric acid solution. H_3PO_4 can be inserted effortlessly into the BCN powder's layer structure and selectively linked to the chain nitrogen atoms via Brønsted acid-base interaction. The oxidized PCN sheet demonstrated a porous morphology, resulting in an improved photocatalytic efficacy. Thin nanosheets displaying a fold structure are visible in Figure 7b,c. whereas Figure 7d–f highlights significant porous structure. Moreover, the two porous nanosheets evaluated comprise solely of three C and N layers (Figure 7g). Although the chemical peel approach offers stable dispersion and a generous surface area for g-C_3N_4 nanostructures, it poses challenges such as low production, usage of corrosive reagents and environmental hazards.

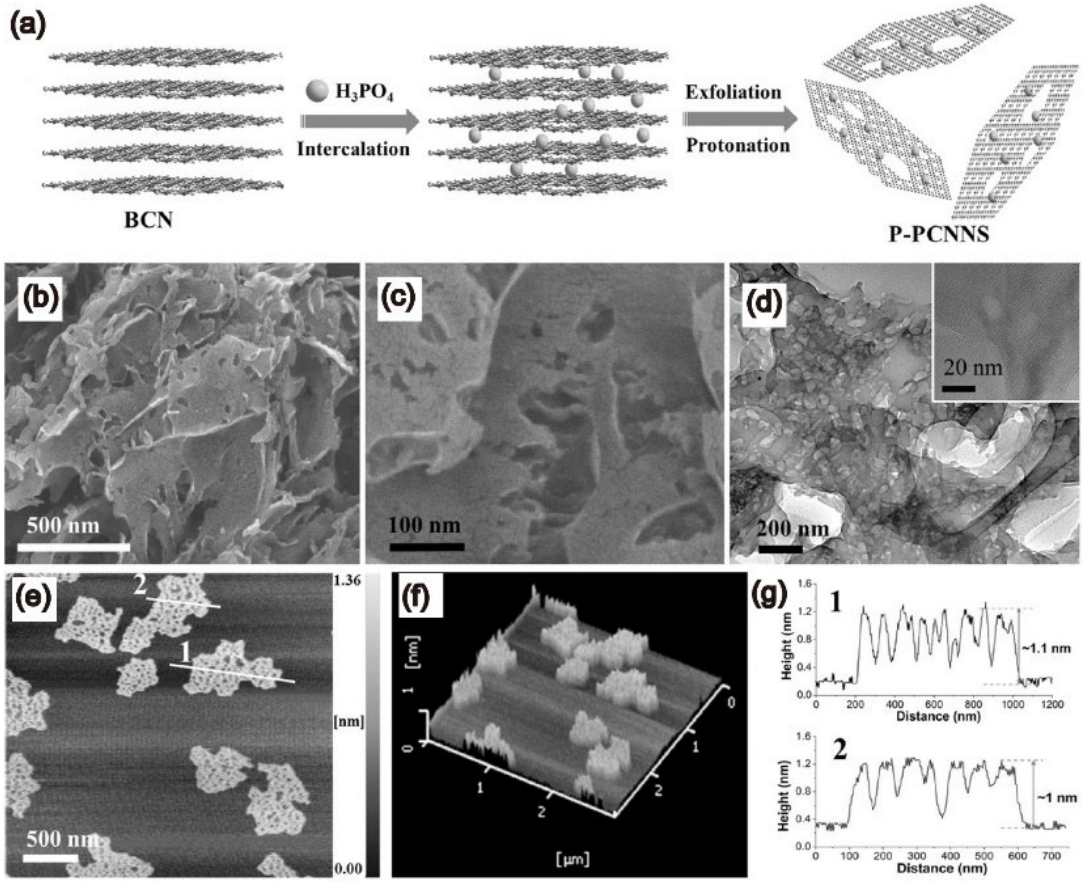

Figure 7. (**a**) Illustration of the preparation process of P-PCNNS; (**b, c**) SEM images of P-PCNNS; (**d**) TEM and HRTEM images of P-PCNNS; (**e–g**) AFM and corresponding height images of P-PCNNS. Figures taken with permission from reference [55].

2.2.2. Thermal Oxidation

Hmmers' method facilitates the separation of graphite into suingle or large-scale layers of graphene. Researchers have attempted to employ the method to prepare g-C_3N_4 nanosheets due to the comparable structure of g-C_3N_4 and graphene. The first report of the thermal oxidation etching of the bulk g-C_3N_4 in air was made by Niu et al. [56], which resulted in the formation of nanosheets with a thickness of approximately 2 nm. However, with the formation of the sheet structure, a large number of interface defects were formed, which reduced the photocatalytic activity. Therefore, the preparation of PCN by thermal oxidation requires other treatments such as atmospheric assistance and chemical stripping. A successful preparation of PCN through thermal oxidation and chemical stripping was demonstrated by Cui et al. [57] Figure 8a illustrates the combination of g-C_3N_4 with a sodium hypochlorite (NaClO) solution, followed by a heating process. This resulted in the synthesis of BCN through the oxidation effect of ClO^- and the intercalation effect of Na^+. Subsequently, a porous structure was created by chemical stripping. XRD and FTIR data (Figure 8b,c) demonstrated that NaClO could be easily removed to form clean g-C_3N_4 nanosheets, which greatly improved the photocatalytic activity of g-C_3N_4. Furthermore, g-C_3N_4 subjected to NaClO treatment exhibits exceptional photocatalytic hydrogen evolution under visible light.

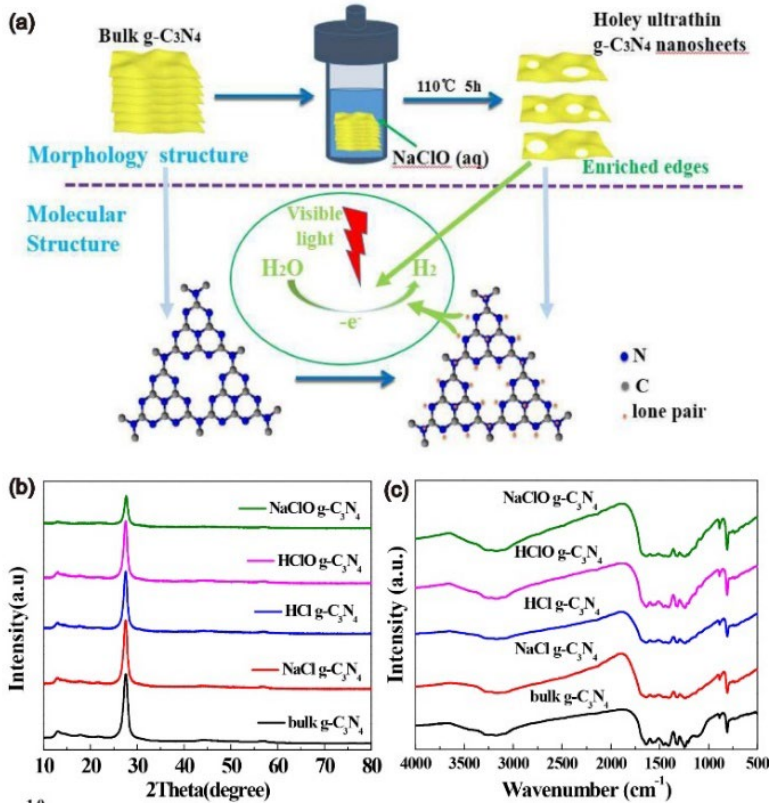

Figure 8. (**a**) Schematic illustration of the NaClO hydrothermal exfoliation of bulk g-C_3N_4 into a single layer, molecular structure models of bulk g-C_3N_4 (left) and exfoliated g-C_3N_4 (right) and proposed mechanism for the photocatalytic H_2 evolution; (**b**) XRD patterns; (**c**) FT-IR spectra of the five products. Figures taken with permission from reference [57].

The preparation of PCN by thermal oxidation and chemical corrosion has the advantages of low cost and easy scalability, but it destroys the structure of the PCN and the reaction process may cause environmental damage. Additionally, this top-down approach typically necessitates a high-quality piece of g-C_3N_4 as a precursor, and the synthesis procedure is intricate [58]. It is important to note that while top-down approaches can exfoliate bulk materials into UCN, the thinnest materials may not necessarily be the best. Furthermore, the self-assembly process of PCN, implemented via the supramolecular method, is facile and straightforward. Should the solvent mitigate challenges posed by the supramolecular self-assembly technique, it could prove to be an effective method for generating micro- and nanostructured materials.

3. Modification Approach

PCN is frequently employed as an exemplary photocatalytic material due to its distinct structure and exceptional intrinsic features. With the continuous research of scientists, the photocatalytic performance of porous carbon-based photocatalytic materials is gradually improved [59]. In this section, we focus on the morphology of PCN and the effect of the basic modification on its photocatalytic performance.

3.1. Morphological Structures

Currently, various methods have been devised to enhance the photocatalytic energy of PCN, surface morphology and adjusting the structure is one of the effective methods [60]. This section introduces the photocatalytic properties of PCN with various nanostructures. The influence of different morphology on PCN was analysed by investigating the formation mechanism of different nanostructures. Exploring more potential PCN structures may be beneficial.

3.1.1. Nanotube Structures

The porous structure of nanoscale pipe piles has the potential to enhance their physicochemical and optical properties, which can result in improved efficiency for photocatalytic applications [61,62]. In recent years, a collection of one-dimensional g-C_3N_4 nanotubes has been reported by researchers. Nonetheless, those reports were

either challenging to create or merely showed reasonable photocatalytic activity, which did not fulfil our expectations [63]. Really, Wu et al. [64] developed a new method for one-dimensional P-doped g-C_3N_4) nanotubes. Figure 9a shows the different porous P-doped g-C_3N_4 tubes prepared by pyrolytic freeze-drying. Dicyandiamide is the precursor of g-C_3N_4 and phytic acid is the morphology regulator. With phytic acid added (Figure 9b–e and Figure 9g–i) the mechanism of PCN synthesis was studied. The morphology of g-C_3N_4 gradually changed from a hollow tube structure composed of nanosheets to a flower-like structure. Phytic acid plays a key role in the adjustment of morphology. The H_2 evolution of PCNT-3 is the highest (2020 μmol g^{-1} h^{-1}), which is 22.4 times that of g-C_3N_4. It can be seen that introducing porous structure while constructing nanotubes is an effective strategy to improve photocatalytic performance.

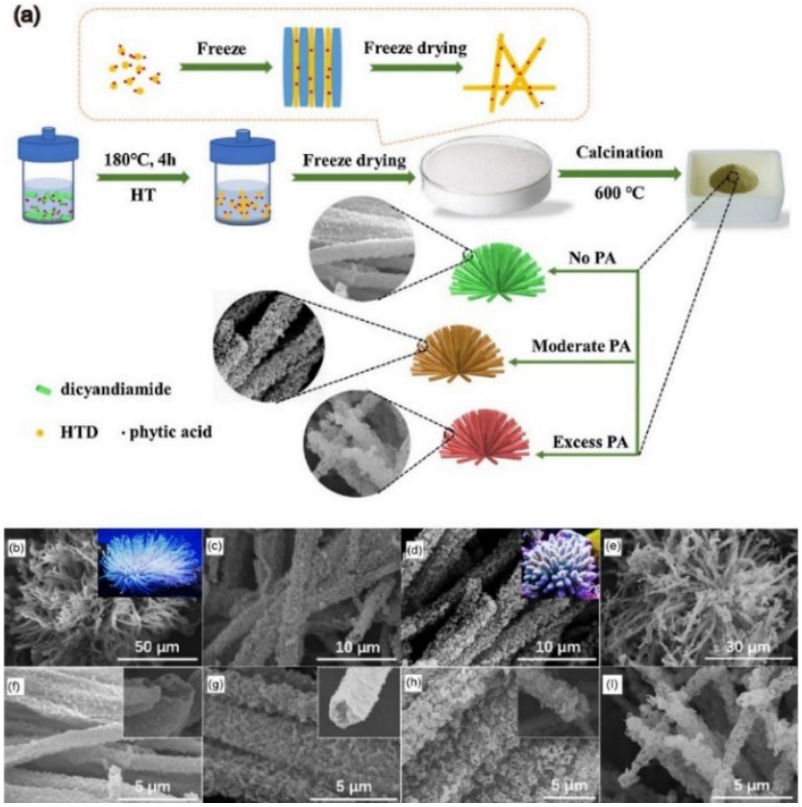

Figure 9 (**a**) Schematic illustration for the formation of 3D porous P-doped g-C_3N_4 tubes. Typical SEM images of (**b,f**) TCN, (**c,g**) PCNT-1, (**d,h**) PCNT-3 and (**e,i**) PCNT-4 samples. Figures taken with permission from reference [64].

3.1.2. Nanosheet Structures

Two-dimensional (2D) nanomaterials possess noteworthy potential within the field of photocatalysis owing to their heightened specific surface area, exceptional chemical stability and electrical conductivity, in conjunction with their exceptional physical properties [65]. In recent years, 2D graphene have shown great potential in the field of photocatalysis due to its superior thermal conductivity, high carrier mobility and large specific surface area [66]. g-C_3N_4 possesses a band gap of 2.7 eV, making it suitable for application in the visible light range up to 460 nm. However, it has an accumulation structure and a specific surface area of only 10 m^2 g^{-1}. There exist certain deficiencies in the advancement of photocatalysis. The creation of 2D g-C_3N_4 tablets is an effective method for modifying g-C_3N_4 [67]. Thus far, researchers have devised techniques such as thermal oxidation, chemical etching, ultrasonic stripping, and supramolecular self-assembly to prepare g-C_3N_4 nanosheets. Supramolecular self-assembly techniques have garnered significant attention due to their uncomplicated operation and no template requirement. Wen et al. [68] using uracil mediated molecular self-assembly strategy, successfully prepared C-doped PCN with melamine and triuric acid as raw materials. The production process is shown in Figure 10. Melamine, tripartite cyanuric acid and uracil are regenerated in deionized water and self-assembled into supramolecular structures by hydrogen bonding. According to the addition of different amounts of uracil to produce different structure of products. The results show that the C–C=C structure of uracil can be introduced into the g-C_3N_4 skeleton to obtain a new type of porous C-doped g-C_3N_4. The specific surface area of g-C_3N_4 increases from 20 to 83.6 m^2 g^{-1}.

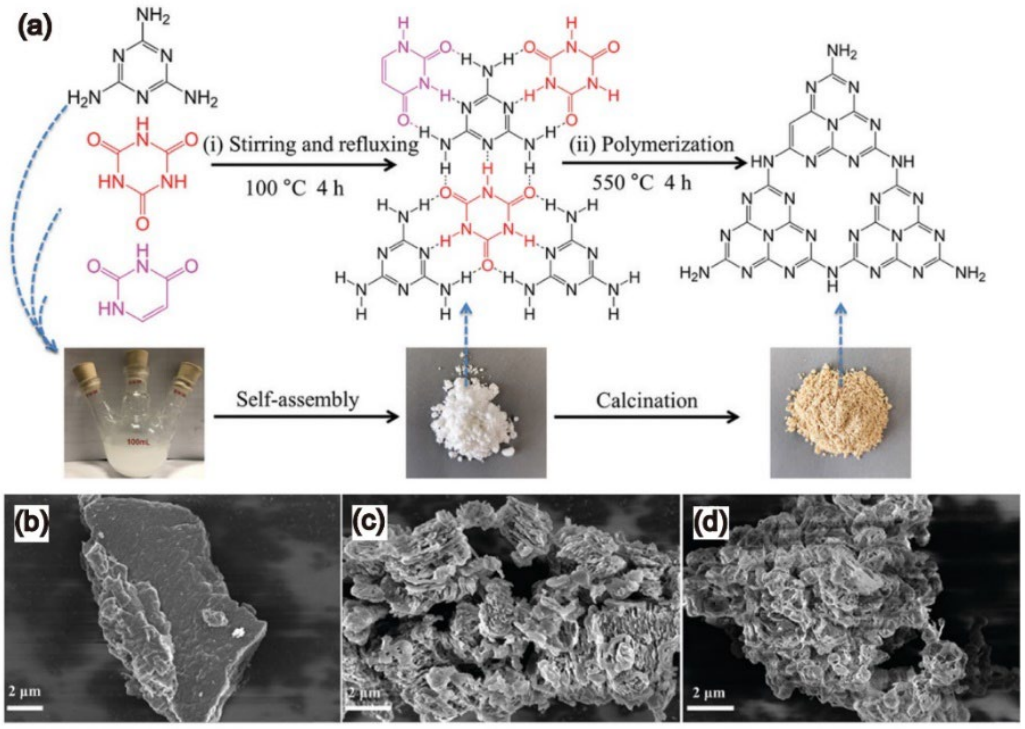

Figure 10. (**a**) Schematic preparation of porous C-doped g-C_3N_4 MCA-U. SEM images of (**b**) g-C_3N_4, (**c**) MCA and (**d**) MCA-U2. Figures taken with permission from reference [68].

3.1.3. Nanosphere Structures

Although 2D g-C_3N_4 nanosheets are considered to be a new type of nanomaterials to meet specific needs. However, due to the strong van der Waals forces between the nanosheets, the structure accumulation and agglomeration are still inevitable, thus reducing the specific surface area. The discovery of 3D structure PCN not only has a large specific surface area, but also can be used as a supporter to prevent nanosheet agglomeration and provide a way for electron transmission [69]. Whang et al. [70] successfully synthesized a series of 3D layered porous carbon/graphite carbon nitride (3D C/g-C_3N_4) composites assembled by nanosheets through the impregnation chemical reduction strategy. The synthesis method is shown in Figure 11a. The obtained samples have interconnected porous networks, which are favorable for multiple reflection and utilization of light. The obtained 3D C/g-C_3N_4 composite has higher hydrogen production rate and stability than the original g-C_3N_4. Chen et al. [71] successfully constructed 3D porous graphite g-C_3N_4 assembled from highly crystalline ultra-thin nanosheets (3D g-C_3N_4 NS) (Figure 11b). On g-C_3N_4 NS-2, the average precipitation rates of H_2 and O_2 are 101.4 and 49.1 μmol g^{-1} h^{-1}, respectively, about 11.8 and 5.1 times of g-C_3N_4 and g-C_3N_4 NS.

The mechanisms of improving the photocatalytic activity of PCN are different for various morphologies and structures. For instance, PCN in the shape of nano-rods widens the area of visible light absorption, while nano-sheet PCN narrows the bandwidth. On the other hand, micro-spherical PCN is more conducive to electron transition. The appropriate carbon nitride pore shape should be selected based on the specific requirements.

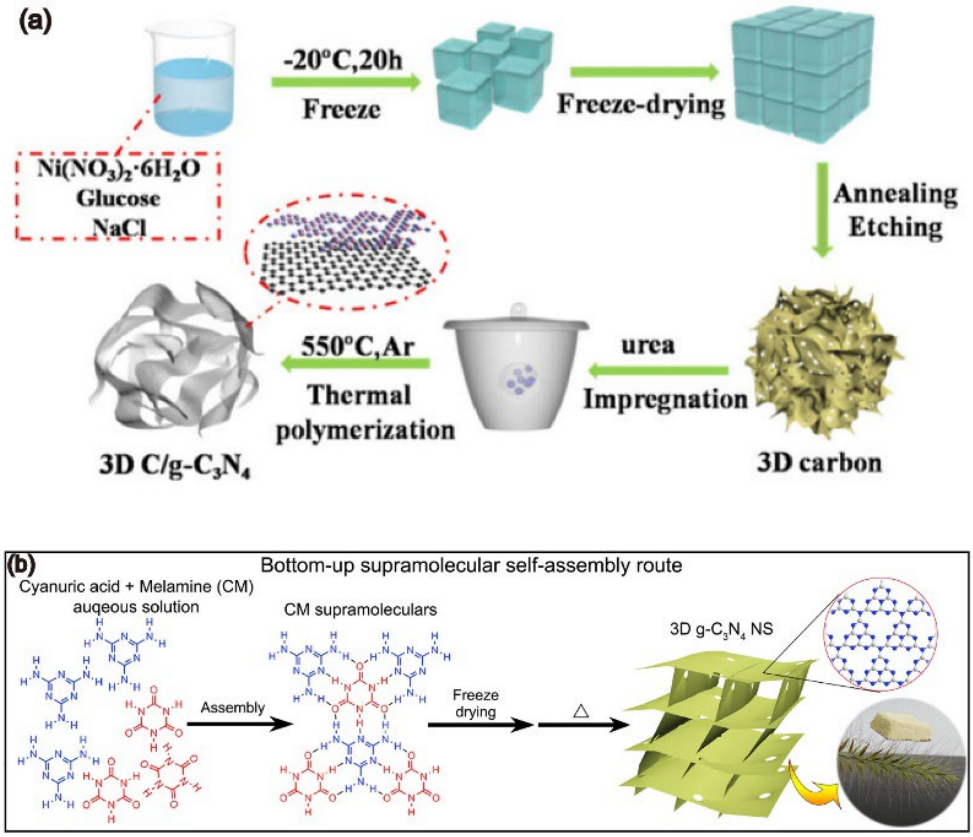

Figure 11. (**a**) Schematic illustration of the synthesis process of 3D C/g-C_3N_4 composites; (**b**) Schematic illustration of the bottom-up supramolecular self-assembly route for synthesizing 3D g-C_3N_4 NS. Figures taken with permission from reference [70,71].

3.2. Functional Modification

Studies indicate that the photocatalytic activity of the modified photocatalyst is better than that of the original photocatalyst. For example, the introduction of defects on the photocatalyst surface can increase the number of active sites on the photocatalyst and doping some elements can widen the absorption edge of photocatalyst. The formation of heterojunction can accelerate the migration of photogenerated electrons. In this section, we will describe the functional modification of PCN, including the introduction of structural defects, element doping and the formation of different heterojunctions.

3.2.1. Defects

The photocatalytic activity of g-C_3N_4 is limited by the separation and transfer rate of photogenerated carriers. The incorporation of surface defects can serve as the surface separation hub of photogenerated carriers to curb their recombination and boost the photocatalytic activity [72–74]. For example, Yang et al. [75] synthesized PCN with the prepared melamine sulfate as the precursor. The resulting samples possess an ample amount of N defects and a porous structure. This has effectively inhibited rapid electron-hole recombination, extending the duration of visible light response. The N defects of melamine sulphate were adjusted by changing the heating rate or extending the pyrolysis time. It is proved that both the low heating rate and the long pyrolysis time led to the increase of defects in g-C_3N_4, which results in the red shift of the light absorption edge of g-C_3N_4. The outcomes indicate that the photocatalytic efficacy of g-C3N4 with a greater number of defects is increased by two times in relation to CN with a high heating rate and short calcination time. The optimal H_2 yield on defect-rich g-C_3N_4 is 905 μmol g^{-1} h^{-1} ($\lambda > 420$ nm).

3.2.2. Element Doping

Element doping is a crucial technique for adjusting the electronic structure of photocatalysts, facilitating the separation and transfer of photogenerated carriers, and broadening the optical absorption range [76,77]. Doping metal atoms (such as Fe, Zn, Cu, and Ag) or non-metallic atoms (such as B, S, O, and I) [78–81] can easily alter the electronic structure of g-C_3N_4 by regulating the band gap of g-C_3N_4 through hybridization of atomic orbital. It

expands its absorbance in visible region, accelerates charge separation, and enhances its mobility, conductivity and photocatalytic activity. This paper introduces the synthesis method of photocatalytic catalyst and the principle of improving photocatalytic performance.

(1) Non-Metal Doping

The surface morphology, particle size, electronic and optical properties and other physicochemical properties can be controlled by introducing non-metallic elements into the PCN framework. The incorporation of non-metal elements extends the absorption of visible irradiation and reduces the recombination of photo-induced electrons and holes. This review focuses on recent progress in the synthesis and design of non- metal doped PCN.

(2) B Doping

B and C exhibit similar size and chemical characteristics. B can replace the carbon atom attached to nitrogen atom in the heptazine unit of g-C_3N_4, and enhance the photocatalytic performance of g through morphology control and electronic structure adjustment. For instance, Wang et al. [82] successfully prepared g-C_3N_4 doped with adjacent nanotubes B through thermal condensation reaction of the precursor and a two-step heat treatment process of pretreatment. Research shows that preheating can enhance the doping of Boron into the precursor and facilitate the formation of adjacent nanotube structures. The synergistic effect of tuning electrons and controlling nanostructures fosters carrier separation and transfer, improving photocatalytic activity.

(3) O Doping

Doping non-metallic elements alters the electronic structure of g-C_3N_4, augmenting its visible light absorption capacity and facilitating segregation of deep optical carrier. The catalytic activity of non-metallic catalysts is influenced by dopants, structural defects, and surface morphology. O doping significantly improves porosity, alters intrinsic electron and band structure, and high carrier recombination enhances light absorption in photocatalytic applications [81]. For example, Long et al. [83] prepared g-C_3N_4 and a series of O-doped C_3N_4 (OCNs) by simple heat treatment and one-step calcination (Figure 12a). The degradation rate of OCN6 was 29 times higher than that of g-C_3N_4 by controlling annealing time. The Figure 12b shows an ordered porous structure. The absorption edge of OCN6 showed a redshift, indicating the narrowest band gap in Figure 12c. The induced O during the modification promoted the formation of O^{2-}, improved the separation efficiency of photogenerated carriers, and inhibited the recombination of h^+ and e^-.

(4) S Doping

S doping can improve the photocatalytic active site of PCN through valence band expansion and shift. Shcherban et al. [76] made S-containing PCN with melamine and sulfuric acid as raw materials. Compared with undoped C3N4 (25 m^2/g), the synthesized material had a higher BET specific surface area (75 m^2/g). The addition of S enhances the light absorption intensity of g-C_3N_4. The synthesized S-doped g-C3N4 is a P-type semiconductor with high catalytic activity for photo reduction of carbon dioxide by water vapor. Research surface that sulfur doping PCN increased the catalytic activity of the reaction by nearly ten times.

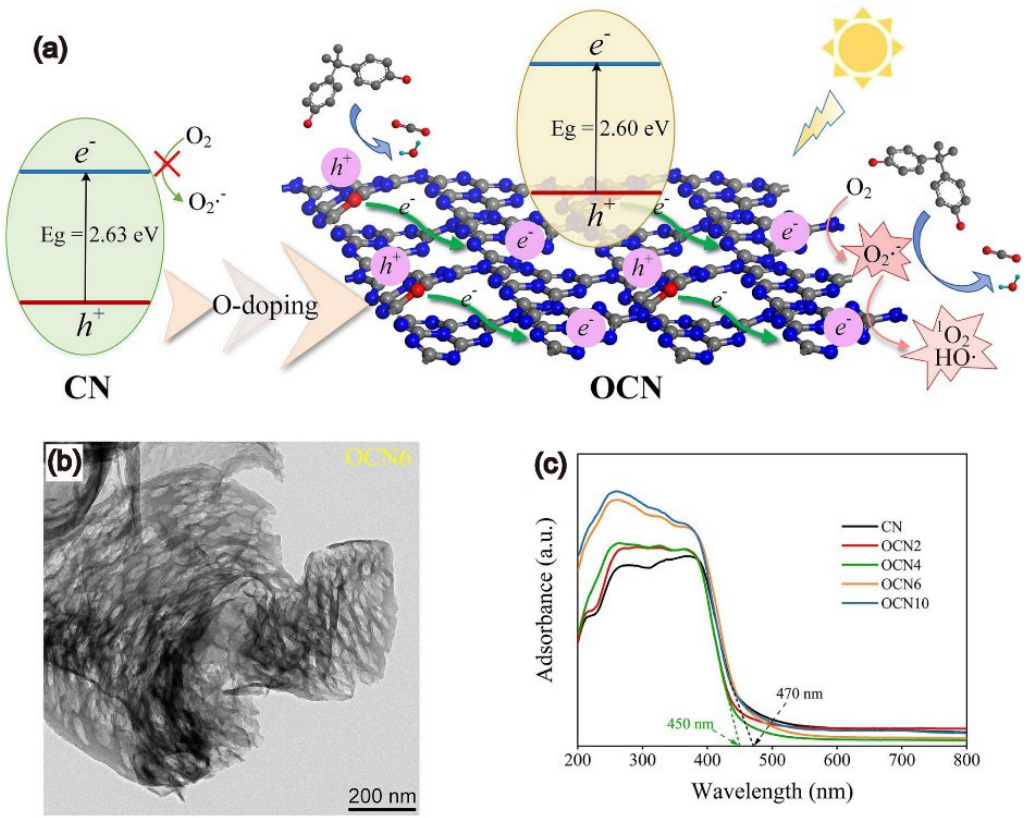

Figure 12. (**a**) Proposed Formation Process of O-g-C_3N_4. (**b**) TEM images of OCN6 (550°C was calcined for 6 h to obtain the product). (**c**) UV-vis diffuse reflectance spectra. Figures taken with permission from reference [83].

(5) P Doping

In recent years, P-doped g-C_3N_4 has become a promising photocatalyst for visible light for hydrogen production and clean environment applications. Liu et al. [84] successfully synthesized P-doped g-C_3N_4 nanotubes by one-step thermal reaction of melamine with sodium hyphosphate monohydrate (NaH_2PO_2 H_2O). The experimental results show that p doping expands the surface area, forming a unique mesoporous structure and forming an amine-rich surface (Figure 13a), P doping reduces the conduction and valence band positions of g-C_3N_4 and narpens the band gap. The electron and hole recombination is proficiently inhibited, resulting in a surge of the adsorption capacity of g-C_3N_4 to 3.14 times. Concomitantly, the yield of CO and CH_4 amplified to 3.10 times and 13.92 times (Figure 13b,c), respectively.

(6) Metal Doping

The recombination rate of photocarriers on the metal catalyst is lower than that on the surface of the non-metal photocatalyst g-C_3N_4. Thus, metal-doped PCN becomes an important research direction. Metal doping can change the band structure of g-C_3N_4, expand the band structure and promote the separation of photogenerated carriers. For example, Reddy et al. [85] prepared V doping g-C_3N_4 nanostructures by direct calcination of urea and ammonium metadadate. Electrochemical impedance spectroscopy measurements reveal carrier dynamics. V doping has a higher photocurrent density than the original g-C_3N_4. Viet et al. [86] prepared Ag-doped g by thermal condensation. The results show that Ag doping not only reduces the band gap energy of g-C_3N_4 but also promotes the formation of photoinduced e^- and h^+ pairs. Metal doping has a certain effect on the photocatalytic performance at the atomic/electron level. Yan at all, [87] synthesized Ru doped PCN (CNRu) using a one-pot heat method. The resulting CN-Ru was found to effectively activate peroxymonosulfate (PMS) and degrade diclofenac (DCF) through a non-free radical patyway. The coordination of Ru to pyridine nitrogen in the form of Ru-N bonds results in high dispersion of Ru. The electron defect transfer between Ru and N facilitates the evolution of the superoxide radical ($O_2^{\bullet-}$). This radical is further hydrolyzed to singlet oxygen ($^1O_2$), which is responsible for the removal of diclofenac. Therefore, the CNRu/PMS system exhibits a high tolerance to inorganic anions, which is conducive to the degradation of DCF.

Element doping is primarily aimed at improving the bandwidth structure and surface photoelectron transfer efficiency of photocatalytic materials. Effective doping strategies can reduce the band gap, accelerate the electron-

hole transfer rate, and improve the photodegradation rate. However, the doping mechanism and the location of certain elements, such as P and certain metal elements, are still unclear and require further study.

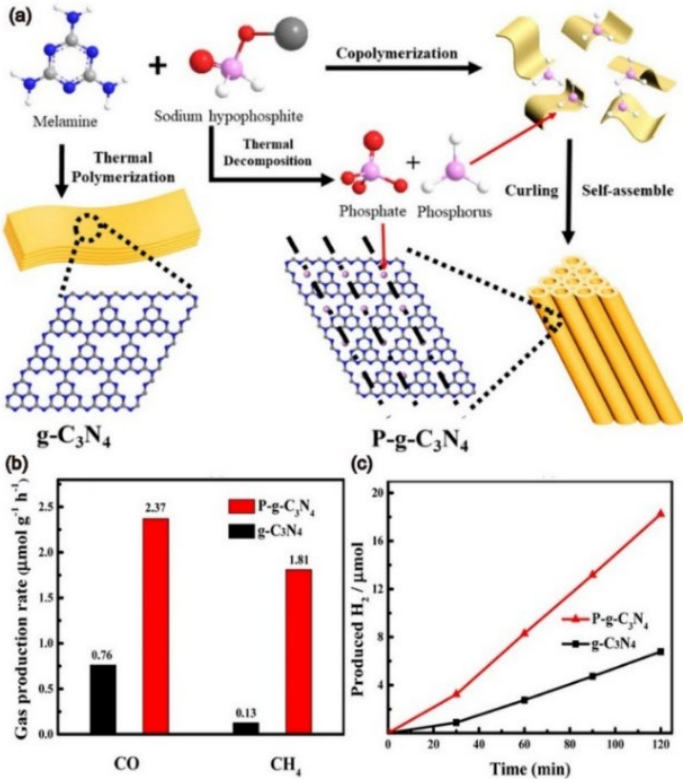

Figure 13. (**a**) Proposed Formation Process of P-g-C3N4. (**b**) Cas production rate of different samples. (**c**) Hydrogen production rates of different samples. Figures taken with permission from reference [84].

3.3. Hybridization

The original g-C_3N_4 absorption has limited photocatalytic performance below 460 nm. The main reasons are insufficient use of visible light, bad charge recombination and limited electron conductivity. Various morphologies and structures can affect the photocatalytic activity. The photocatalytic activity was significantly enhanced through element doping. The introduction of O can disrupt the symmetry of g-C_3N_4 and facilitate the separation of electron and hole pairs. In addition, structural imperfections can offer additional active sites for promoting the separation of photocarriers. Combining the modified PCN with other materials may enhance the photocatalytic performance. This chapter mainly introduces the influence of hybrid mode on PCN photocatalyst. Hybridization is an important method to promote photogenic carrier separation. Hybridization strategies of PCN are divided into two types. The first is hybridization of PCN with cocatalyst, and the second is hybridization of PCN with photocatalyst. The two strategies work slightly differently. The mechanism of the PCN cocatalyst is as follows: upon visible light irradiation, the PCN is excited, resulting in the transfer of electrons and holes. The co-catalyst's superior conductivity and storage capability enable it to accelerate the transfer of photogenerated electrons at the interface, thereby accelerating the separation of photogenerated e^- and h^+. The hybridization of PCN and photocatalyst can be divided into three types: n-n heterojunction, p-n heterojunction and Z-type heterojunction. The mechanism of n-n heterojunction is similar to that of P-heterojunction. Under light, the two photocatalysts are stimulated to produce photoelectrons. Electrons are transferred from the catalyst with low conduction band to the catalyst with high conduction band, and holes are transferred from the photocatalyst with high conduction band to another photochemical agent, resulting in effective separation of electrons from hole pairs. The photogenerated electrons in the Z-scheme heterojunction migrate from the conduction band potential catalyst to the lower valence band potential photocatalyst. Thus, photogenerated e^- and h^+ can be effectively separated.

3.3.1. p-n Heterogeneous Junctions

Constructing p-n junction is an effective strategy to enhance photocatalytic activity [88–92]. g-C_3N_4 is a typical N-type photocatalyst, because the electron concentration in its structure is greater than the hole

concentration. N-type g-C_3N_4 combined with P-type photocatalyst (h^+ concentration is greater than e^- concentration) to form n-p heterojunction, thus promoting the separation of e^- and h^+ pairs. Paramanik et al. [93] synthesized a Boron-doped rGO/$PbTiO_3$ p-n heterojunction through a convenient and straightforward hydrothermal method. Figure 14 shows that the introduction of P-type broadens the visible light absorption range of PCNS. The formed heterojunction accelerates the transfer of photogenerated electrons from g-C_3N_4 and promotes the separation of photogenerated carriers. B-rGO/$PbTiO_3$ junction photocatalyst improved the photoreduction of H^+ to H_2 gas under visible light irradiation. The photocatalyst exhibits a hydrogen decomposition rate of 293.79 μmol h^{-1}, with excellent cyclic stability and energy conversion efficiency.

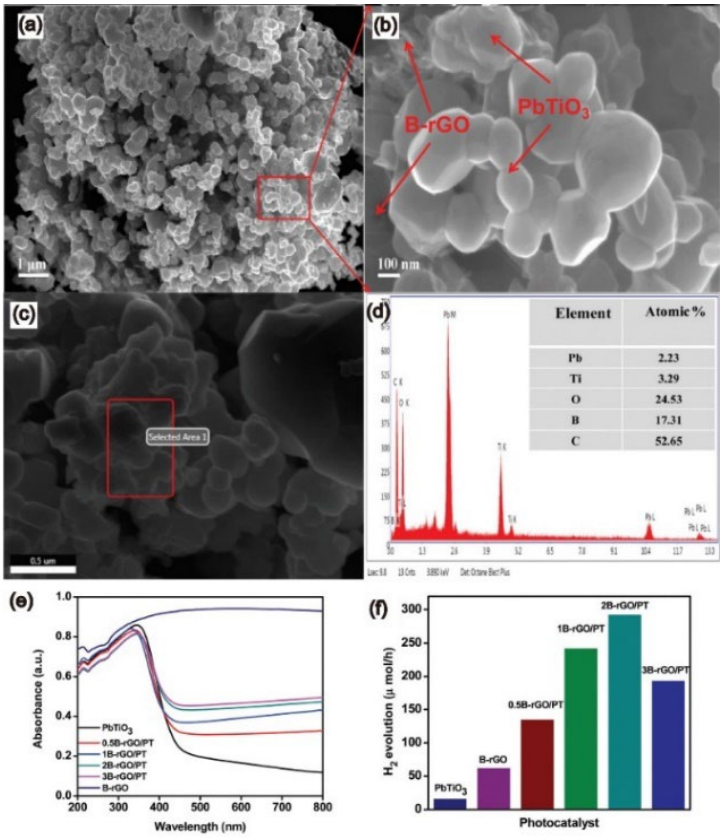

Figure 14. (**a,b**) 2B-rGO/PT; (**c,d**) EDX spectrum of the p–n heterojunction (the inset shows the elemental composition of each element); (**e**) UV-Vis DRS spectra of the series of B-rGO/$PbTiO_3$ heterojunctions; (**f**)Photocatalytic H_2 evolution of the series of B-rGO/$PbTiO_3$ heterojunctions. Figures taken with permission from reference [93].

3.3.2. n-n Heterogeneous Junctions

Consisting of two photocatalysts (let be PC l and PC ll). Under the condition of photoexcitation, the photogenerated e^- are transferred from PC I to PC II, while the photogenerated h^+ are transferred in the opposite direction, and the electrons and holes are effectively separated in space. Hao et al. [94] using titanium tetrachloride ($TiCl_4$) and melamine as precursors, the obtained samples were labeled as TC_X by changing the amount of melamine. The g-C_3N_4/TiO_2 n-n heterojunction composites with high specific surface area were prepared by simple in-situ hydrothermal synthesis and calcination. As shown in Figure 15, titanium dioxide was followed by g-C_3N_4, and the absorption intensity of TC_3 sample was increased and extended to the visible region. The formation of n-n heterojunction enhanced the photodegradation ability. TC_3 samples showed the highest photocatalytic performance, 18.7 and 3.5 times higher than pure TiO_2 and g-C_3N_4, respectively.

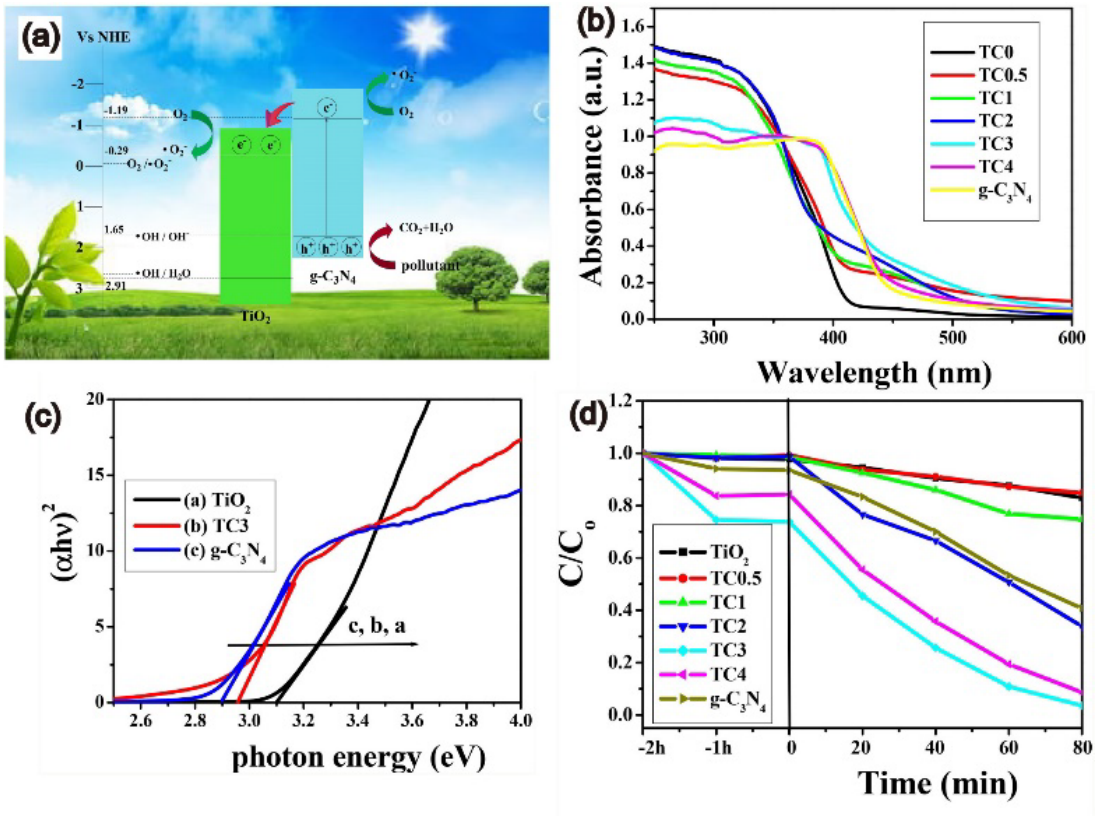

Figure 15. (**a**) Photocatalytic mechanism of TC_3 heterojunction catalyst under visible light irradiation; (**b**) UV-vis diffuse reflectance spectra of the as-prepared g-C_3N_4, pure TiO_2 and TC3 heterojunction photocatalyst. (**c**) The band gaps of as-prepared g-C_3N_4, pure TiO_2 and TC_3 heterojunction samples determined from the plots of versus photon energy. (**d**) Photocatalytic performance of pure TiO_2, g-C_3N_4 and TCx catalysts on the decolorization of RhB under visible-light irradiation ($\lambda > 420$ nm). Figures taken with permission from reference [94].

3.3.3. Z-Scheme Heterogeneous Junctions

The migration pathway of photogenerated electrons may alter when some heterojunction photocatalysts utilized for degradation are incapable of generating adequate oxidation intermediates owing to the existence of VB potential. The photogenerated electrons retained in the PC I conduction band and the holes in the PC II valence band will participate in the reduction and oxidation reactions respectively, thus forming the Z-type heterojunction [95–99]. As shown in Figure 16, Chouchene et al. [100] prepared for the first time a novel Z-heterostructure photocatalyst combining g-C_3N_4 with $SmFeO_3$ by solvothermal and ultrasonic mixing methods. A good contact interface is established between g-CN and $SmFeO_3$. Therefore, the interface carrier can be effectively separated, shortening the charge transport pathway. The capture experiments of photodegradation active substances showed that $\bullet O_2^-$ free radicals and holes played the main roles. The formation of Z-type heterojunction is beneficial to promote the separation of photogenerated carrier and enhance the REDOX capacity of g-CN/$SmFeO_3$ composite photocatalyst.

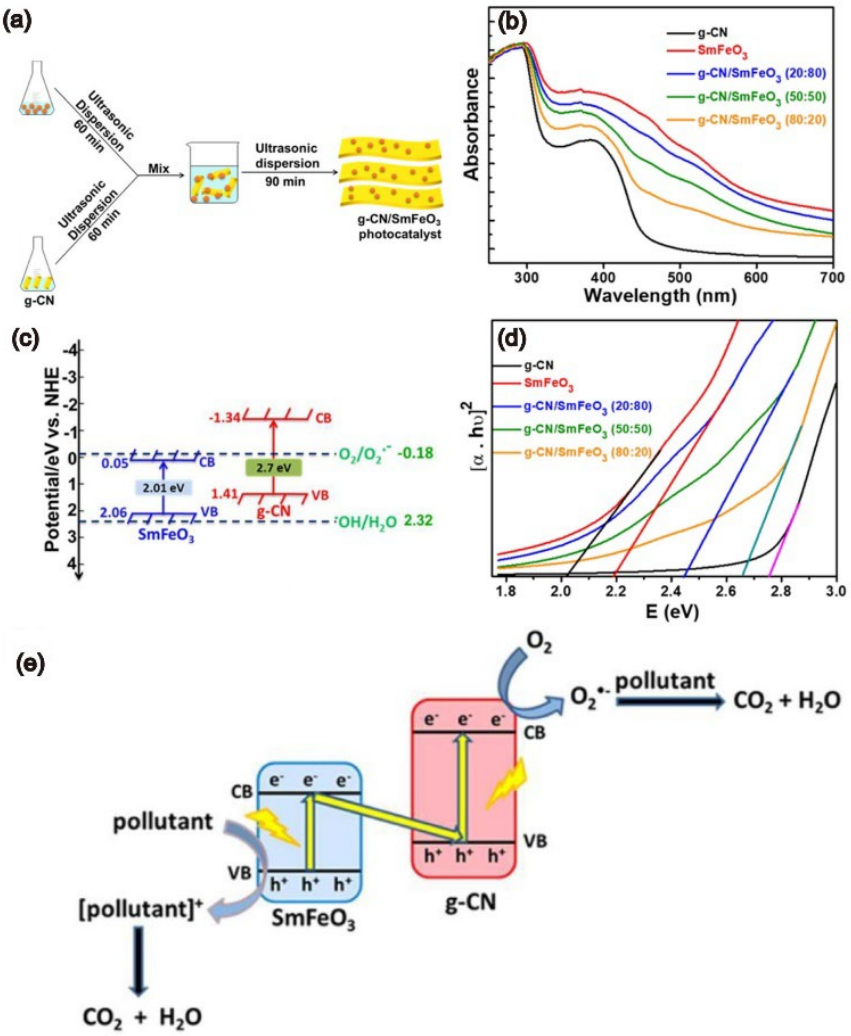

Figure 16. (**a**) Schematic representation of g-CN/$SmFeO_3$ composites synthesis; (**b**) UV-visible absorption spectra of bulk g-CN, $SmFeO_3$ and g-CN/$SmFeO_3$ photocatalysts PL emission spectra; (**c**) Band structure of the g-CN/$SmFeO_3$ photocatalyst; (**d**) the corresponding $[\alpha hv]^2$ *vs* photon energy plots; (**e**) schematic illustration of the delocalization of charge carriers and of the formation of reactive species involved in the photodegradation. Figures taken with permission from reference [94].

4. Antibiotic Degradation Applications

Recently, the use of antibiotics has made remarkable progress in the treatment of infectious diseases and agricultural production [101]. However, the overuse and abuse of antibiotics have produced a large amount of harmful wastewater, causing great harm to the environment [102]. Antibiotics are widely used in the treatment of microbial infectious diseases [103]. Antibiotic residues can provide a favorable environment for drug-resistant bacteria and drug-resistant genes to multiply and spread which poses a serious threat to human and animal health. Antibiotic resistance is one of the major health tests of the 21st century. Therefore, an efficient method to remove its residue is urgent. Traditional effective removal methods including precipitation [104], filtration [105], and coagulation [106] are relatively inefficient and cannot effectively remove antibiotic residues. At present, new technologies based on adsorption [107], advanced oxidation [108], and photocatalytic degradation [109,110] have been reported. Photocatalysis is considered as the most effective method to treat antibiotic wastewater because of its high degradation rate and no pollution. Among many photocatalysts, g-C_3N_4 has attracted more and more attention owing to its advantages such as low cost, good chemical stability, wonderful visible light responsiveness, and reusable. However, due to the problems such as small specific surface area, rapid photocarrier recombination and narrow visible light absorption range, the single g-C_3N_4 photocatalytic performance still needs to be improved. In order to increase the specific surface area of the original g-C_3N_4, developing PCN with special structure is a feasible method. As is well-known, PCN has the advantages of narrow band width, satisfactory visible light absorption, excellent absorption capacity for reactant, which can be used as a promising photocatalyst for antibiotic

degradation. Therefore, this section will elaborate on the application of PCN photocatalyst in the degradation of antibiotics such as tetracycline, ciprofloxacin, norfloxacin, etc.

4.1. Tetracycline Degradation

Tetracycline (TC) have been widely used in medicine and clinic [111]. TC is the second most commonly used class of antibiotics in the world, accounting for more than a third of antibiotic production [112]. Additionally, TC is extensively utilised for treating animal illnesses and adding to animal feed in subtherapeutic doses as a preventative measure against animal diseases and to foster animal development. Nonetheless, due to the excessive or inappropriate use of this drug, antibiotics have been accumulating in large quantities in our aquatic environment for a long time. This emerging pollutant can inhibit the growth of bacteria and other aquatic life, posing a serious threat to the ecosystem. At the same time, TC is by far the most frequently used antibiotic in animal husbandry, with the largest production and sales in the world. Which may affect ecological health and safety as agricultural livestock and poultry waste enters the soil environment directly [113]. Interestingly, photocatalyst has become an effective solution to remove and reduce environmental pollutants, owing to its high degradation rate, high mineralization efficiency and low toxicity [114]. The mechanism is that hydroxyl radicals (•OH) and superoxide radical ($\bullet O_2^-$) can break down a variety of antibiotics into less toxic organic matter, while releasing low molecular intermediates CO_2 and H_2O [115]. Among the existing photocatalysts, g-C_3N_4 has a medium band gap of about 2.7 eV. Because of its easy access, absorption of visible light, low cost, non-toxic and other excellent performance, it has attracted growing attention. However, the photocatalytic activity of pure g-C_3N_4 is poor due to the insufficient utilization of visible light and the high recombination rate of photogenerated e^- and h^+. Therefore, the reasonable design and modification of g-C_3N_4 to improve its photocatalytic performance is an urgent requirement, but also a huge challenge. In this section, we summarized the application of PCN for TC degradation, and discussed how to enhance the photocatalytic performance for TC degradation by regulating the morphology and size of PCN.

Primarily, the element-doped PCN photocatalyst can effectively enhance carrier separation due to its unique electronic structure. For instance, Bao et al. [116] successfully prepared Cu-doped 3D PCN (Cu-PCN), self-complementary hydrogen bonds and electrostatic interactions of precursors through supramolecular template-mediated strategies (Figure 17a) disassembled the reactants into the polymers. After light exposure, Cu-PCN is excited to produce hole-electrons, and some excited electrons transition to the electron-deficient Cu surface, realizing the photogenerated carrier separation (Figure 17b). $\bullet O_2^-$ produced by the reaction of electrons with dissolved oxygen can be further combined with H_2O to form •OH (Figure 17c–e). The results show that the Cu-PCN composite has a larger specific surface area (142.8 m^2/g) and enhanced visible light absorption range. This study shows that hierarchical porous structures can be obtained by self-complementary N-H···N, N-H···O hydrogen bonds and electrostatic interactions, which provides a useful strategy for the synthesis of large specific surface area photocatalysts.

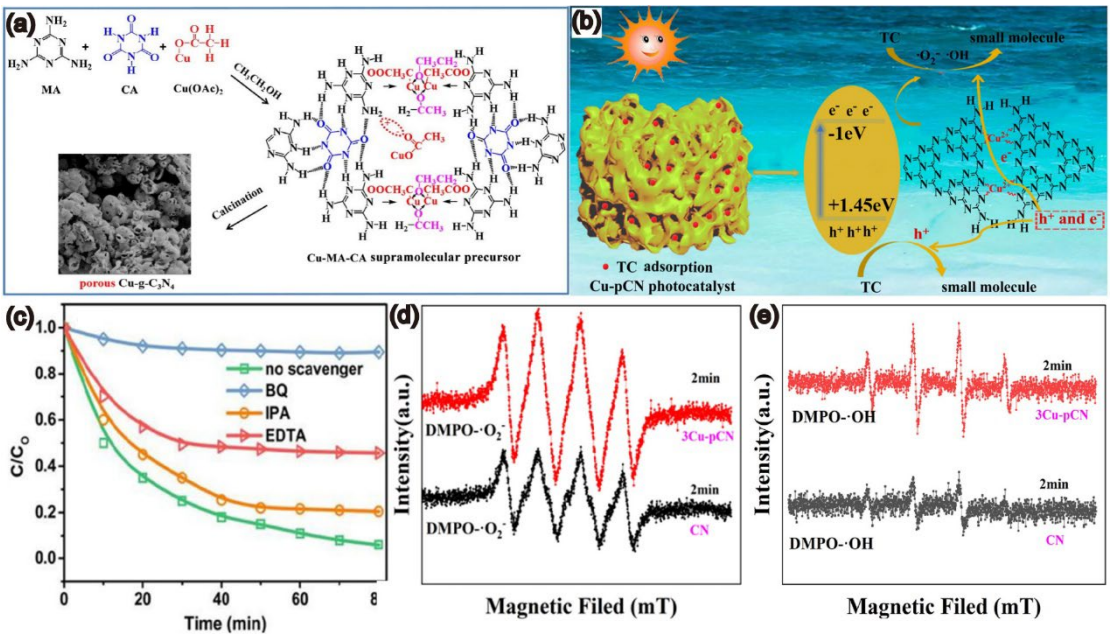

Figure 17. (**a**) Formation process of porous Cu-g-C_3N; (**b**) The mechanism of Cu-PCN on TC degradation; Active species capture experiments (**c**); EPR (**d,e**) of 3Cu-PCN and CN Figures taken with permission from reference [116].

Recently, Zhou et al. [117] grafted a benzene ring with a strong electron-absorbing group (boric acid group) onto CN by a one-pot hot melting method, and thermally induced urea copolymerized with m-aminobenzoborate (APBA) to synthesize B-doped PCN photocatalyst. The photocatalyst not only has a porous nanolayered structure, but also has an ultra-hydrophilic, narrow band gap, and remarkable degradation capacity. It can degrade 81.3% TC (40 mg L^{-1}) within 100 min, which is 6.75 times the original CN. Therefore, it is feasible to construct 3D structure to enhance the photocatalytic performance. N-doped graphene quantum dots (N-GQDs) are known for their high stability, catalytic activity and biocompatibility. Zhang et al. [118] using element doping, N-GQDs coupling and morphological regulation strategies to prepare a novel ultra-thin porous N-GQDs/P-g-C_3N_4 (PG-CNS) nanocomposite. P doping enables the visible response range to extend to more than 780 nm. As shown in Figure 18a–d, light absorption is slightly enhanced in the whole visible or even near infrared range. The introduction of N-GQD enhances electron conduction (Figure 18e,f), and the porous structure provides a shorter migration path. The prepared photocatalyst showed improved photocatalytic performance of TC degradation (Figure 18g,h). N-GQD have unique edge effect, quantum effect, and excellent electrical conductivity, and it is a feasible scheme to combine N-GQD with g-C_3N_4 to form photocatalytic composites with different porous morphology. Quyen et al. [119] prepared sulfur-doped g-C_3N_4 using thio-acetamide as sulfur source and melamine comonomer by heat-sensing copolymerization method. The visible light activity of S-doped g-C_3N_4 on TC degradation is about 97.5%, which is significantly better than the original g-C_3N_4. So far, there are few reports on the decomposition of S-doped g-C_3N_4, which provides a good strategy for our follow-up research.

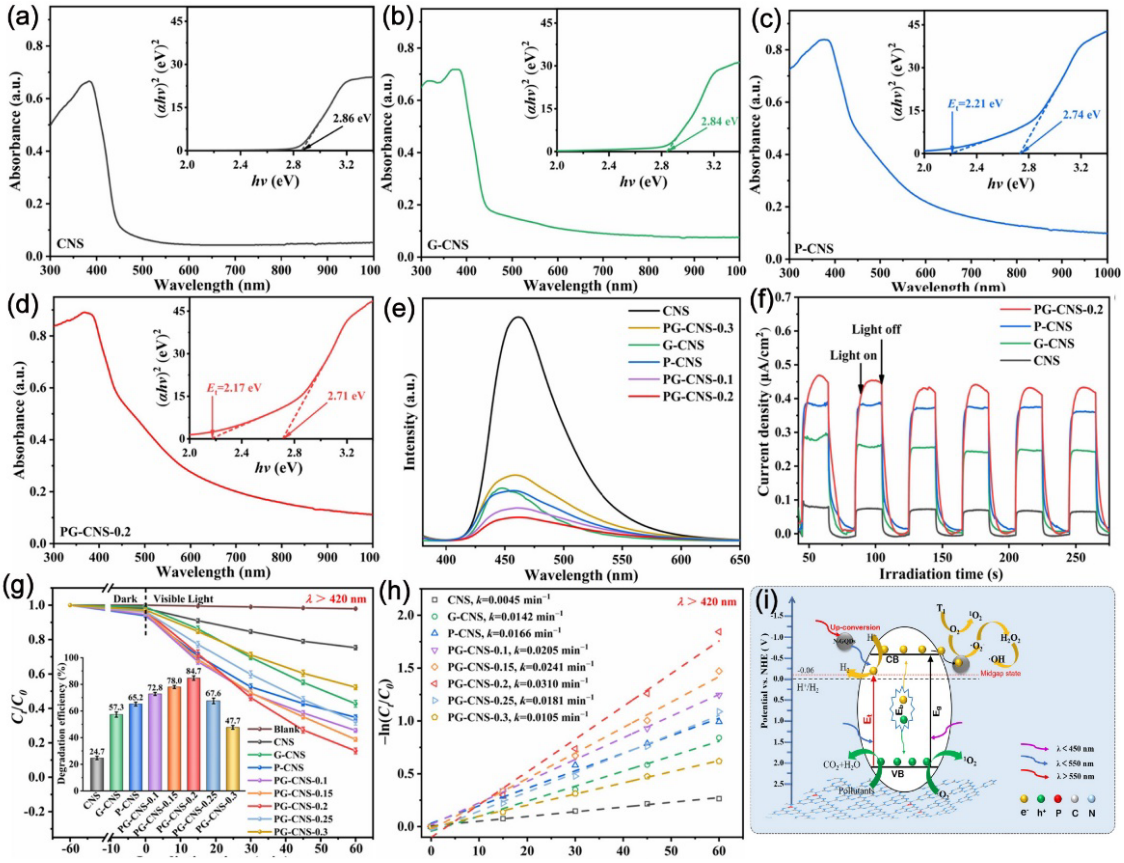

Figure 18. (**a–d**) UV-Vis-NIR DRS (inset: the corresponding bandgap); (**e**) PL time-resolved PL spectra of the samples; (**f**) Photocurrent response of the samples; (**g**) Photocatalytic degradation curves; (**h**) corresponding degradation kinetics of TC; (**i**) Schematic representation of the possible photocatalytic mechanism for PG-CNS-0.2. Figures taken with permission from reference [118].

In addition, defect engineering plays a significant role in g-C_3N_4 for the degradation of TC. Careful control of the distribution and concentration of defect sites may be an effective method to adjust the band gap, surface area and improve the efficiency of carrier inhibition. For example, Zhang et al. [120] synthesized sea urchin g-

C_3N_4 with C vacancy and O doping (SUCN-6) through calcination and hydrothermal synthesis. Figure 19b,c showed that the sea urchin structure. After synthesis, the band gap becomes narrower with higher valence band, which enhanced the oxidation capacity for TC degradation. The generation of C vacancy can optimize the surface atomic arrangement and regulate the electron configuration, promote the charge carrier transport and reduce the electron-hole pair recombination, effectively accelerate the carrier separation and transfer (Figure 19h,i). Under visible light, SUCN-6 showed a TC removal efficiency of approximately 89% within 20 min. Surface atomic properties are a promising strategy for improving electron-hole pair separation. This study optimizes the structure of SUCN-6 by optimizing the surface atomic properties, thereby improving the electron hole separation ability and providing an excellent structural modification strategy.

At the same time, template method is an effective strategy to form porous structure. For instance, Preeyanghaa et al. [121] synthesized multistage CN nanorods with carbon vacancies by ultrasound-assisted thermal condensation using melamine HCl complex as template. The photocatalytic degradation efficiency of TC was significantly improved within 60 min, which reached 100%. One-dimensional g-C_3N_4 is limited by the surface area, the active site is low, and the construction of layered CN structure is a promising solution.

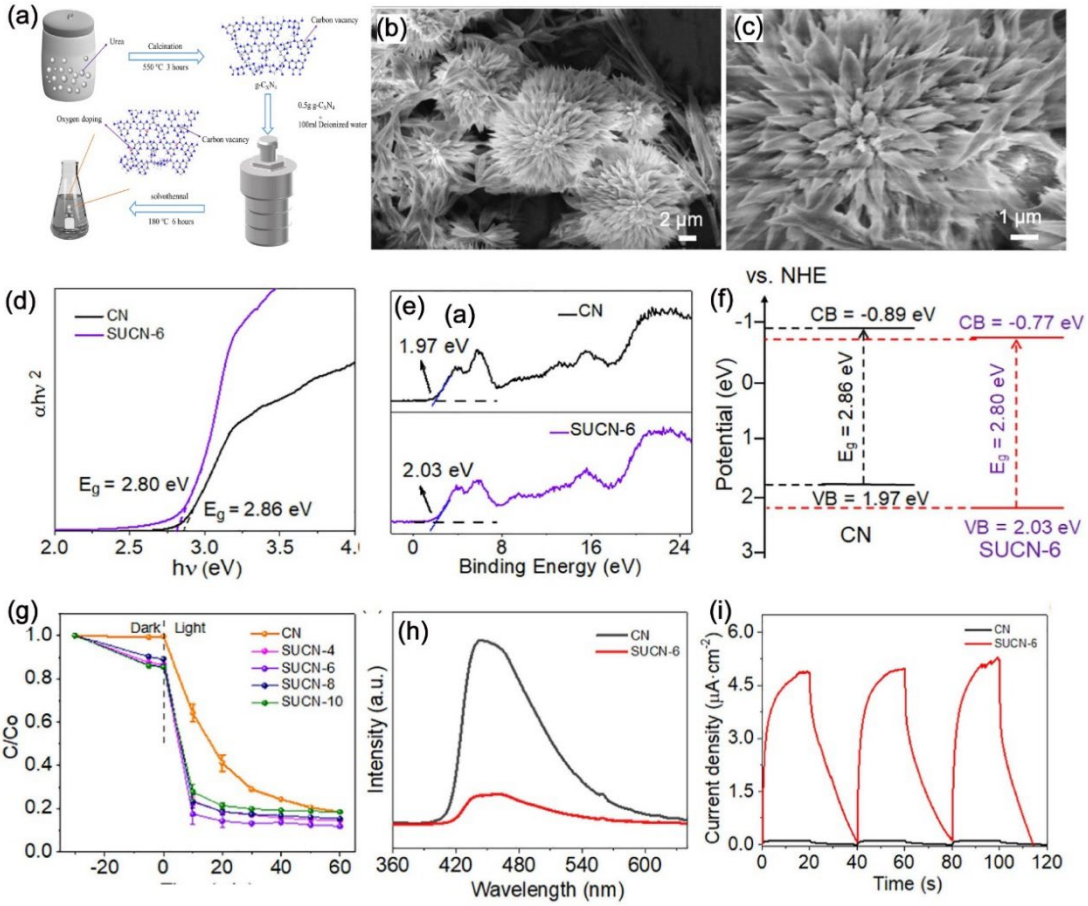

Figure 19. (**a**) Schematic illustration of the preparation of SUCN-6 via thermal condensation followed by hydrothermal treatment; (**b–c**) corresponding high-resolution SEM images of SUCN-6; (**d**) corresponding Kubelka-Munk transformed reflectance spectra; (**e**) valence band-XPS scan spectrum and (**f**) electronic band structures of CN and SUCN-6; (**g**) Degradation efficiency towards TC over various photocatalysts under visible light irradiation; (**h**) PL spectra; (**i**) photocurrent responses (TPC) under room temperature. Figures taken with permission from reference [120].

This work provides a method for further experiments by constructing 2D structures to increase the active sites of photocatalytic reactions. However, randomly arranged 2D nanosheets also create a less than ideal surface area. In the process of photocatalytic reaction, the material is easy to aggregate, resulting in the reduction of the active site. Therefore, it is necessary to explore 3D carbon nitride materials with large pores. Ghosh et al. [122] first constructed 2D N-vacancy engineering nanosheets by self-assembly, and then fabricated a novel 3D macroporous g-C_3N_4 skeleton by heat-treating the sheets. The addition of N vacancy changes the electron band structure of photocatalyst and generates a middle band gap platform, thus improving the visible light extraction

ability. Vacancy integration also effectively inhibits electron hole recombination. The presence of large pores in the structure increases the availability of active reaction sites. The macropore structure showed excellent photocatalytic efficiency for degradation of TC antibiotics under LED light. Therefore, the modification of g-C_3N_4 and retrograde 3D morphology is a feasible strategy.

Recent research has indicated that heterojunction photocatalysis is a highly effective and promising approach to enhancing the separation/migration of electron hole pairs and mitigating the effects of TC pollution on aquatic environments. For instance, all-solid Z-type heterojunction has attractive ability in charge separation and transfer. Jiang et al. [123] constructed all-solid terpolymer Z-scheme heterojunction with g-C_3N_4 nanosheets, carbon nanotubes (CNT) and Bi_2WO_6 (BWO) nanosheets, and the degradation of tetroyclines reached 87.65% (Figure 20a–c). The efficient separation of charge carriers induced by the CNT-mediated Z-scheme mechanism mainly contributes to the enhancement of the photocatalytic activity of CN/CNT/BWO heterojunctions (Figure 20d–e). Recently, the construction of all-solid-state Z-type photocatalytic systems based on neural networks has been considered as an effective method, and the success of Jiang et al. provides a reasonable all-solid-state Z-type heterojunction design. Hu and co-workers [124] fabricated g-C_3N_4 from melamine by thermal condensation, and then hydrothermal treatment by adding zinc acetate dihydrate. Spherical zinc oxide (ZnO) nanoparticles were loaded on the surface of g-C_3N_4 for forming ZnO/g-C_3N_4 p-n heterogeneous nanocomposites. ZnO/g-C_3N_4 heterogeneous nanocomposites can effectively reduce the recombination of e^- and h^+, generate more h^+, and degrade 78.4% of TC within 50 min. The preparation of heterogeneous junctions with large interfacial contact areas is an effective technique for developing high performance photocatalysts. Interestingly, it is generally reported that synthesized ZnO/g-C_3N_4 nanocomposites are obtained by simple blending methods, resulting in uneven morphology, difficult to control and practical application. However, this method can control the shape of ZnO to form smaller ZnO nanocrystals to improve the photocatalytic performance, and has broad application prospects. The preparation of heterojunctions with large interfacial contact areas is an effective technique for developing high performance photocatalysts. Wang et al. [125] constructed the S-scheme heterojunction based on tin niobate (SNO) nanosheets and PCN by one-step calcination method. The prepared SNO/g-C_3N_4 composites effectively enhance charge separation ability by constructing internal electric field. The TC degradation efficiency was 1.64 times than that of original g-C_3N_4. This study introduces a novel method for designing and synthesising semiconductor heterojunction photocatalysts.

The degradation mechanism of antibiotics can be revealed through theoretical calculations (DFT). Mateen et al. [126] found that PCN obtained by template-free polymerization of urea and melamine monomers with a TC degradation efficiency of 97.3%. Additionally, DFT calculations revealed that the stronger interaction between the atomic Mo site and O_2 (ads) promotes faster electron transfer, thereby activating O_2 to generate ROS ($\bullet O_2^-$, •OH).

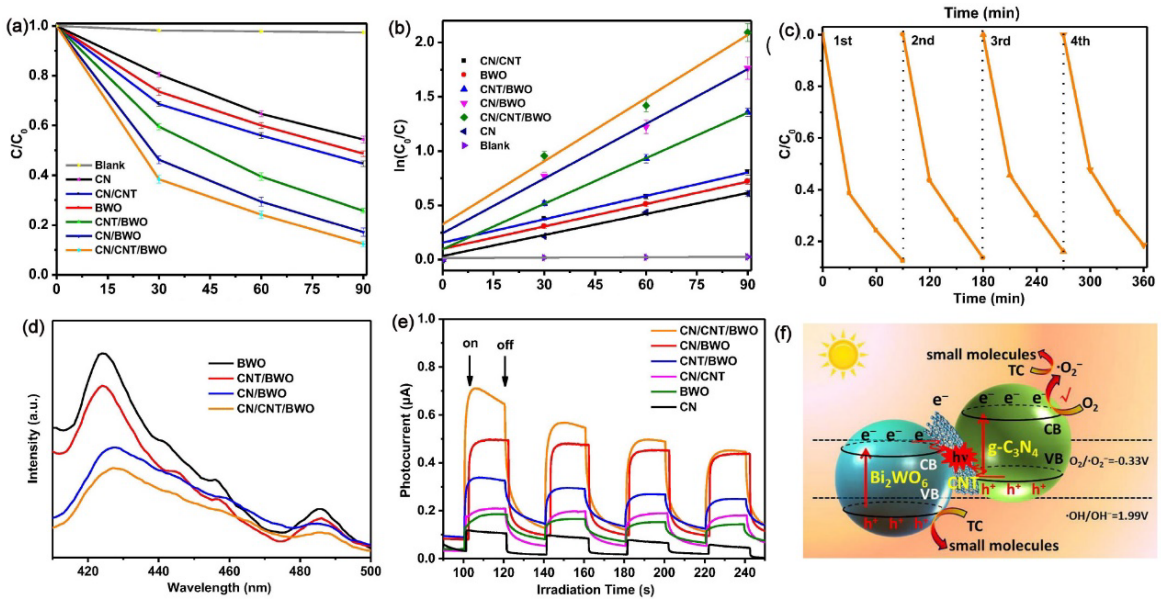

Figure 20. (**a**) Photocatalytic degradation of TC as a function of irradiation time; (**b**) Kinetic curves for TC degradation over the as-prepared photocatalysts; (**c**) Recycling curves of CN/CNT/BWO; (**d**) PL spectra and (**e**) transient photocurrent responses of different as-prepared photocatalysts; (**f**) mechanism of the photo-generated carrier transfer pathways in CN/CNT/BWO under visible light irradiation. Figures taken with permission from reference [123].

4.2. Ciprofloxacin Degradation

Fluoroquinolones have been widely used in veterinary medicine since the 1960s [127]. As a significant member of this group, ciprofloxacin (CIP) is extensively used to treat diseases caused by both gram-negative and gram-positive bacteria. As a result, considerable amounts of CIP and its products have been found in water sources, with concentrations ranging from ng/L to μg/L [128–130]. The presence of this drug in the aqueous medium can increase the stability of the antibiotic, resulting in toxicity and carcinogenic effects. Hence, it is imperative to employ an efficient and eco-friendly technique to address this issue. The common methods to remove CIP from sewage include chemical oxidation, adsorption, flocculation, and reverse osmosis [131,132]. However, these technologies have disadvantages such as high cost, low efficiency, harmful products, and excessive sludge. PCN-based photocatalysts have attracted wide attention for degrading CIP due to its high photocatalytic efficiency.

In general, porosity and nonmetallic doping produce excellent photocatalytic activity by providing a narrow band gap, porous structure, and large specific surface area. For example, using olyoxyethylene stearyl ether as template agent and copolymer, Chuaicham et al. [133] synthesized hollow porous O-doped g-C_3N_4 structure by *in-situ* thermal condensation method. It can be seen from the SEM image that the use of O template makes g-C_3N_4 produce hollow porous structure, and the doped PCN can produce more active free radicals (Figure 21a–d). The photocatalytic CIP decomposition performance was greatly enhanced. As shown in Figure 21e–h, photocurrent response that O doping can reduce the recombination rate by generating new electron trapping states and achieve high charge separation, and thus increasing photocatalytic activity. The optimal samples removed nearly 95% CIP within 20 min and achieved a rate of 0.122 nmin^{-1}. The composite prepared by this method does not need to use hydrofluoric acid, which is harmful to the environment, to remove the template, is environmentally friendly, and has the prospect of large-scale production application.

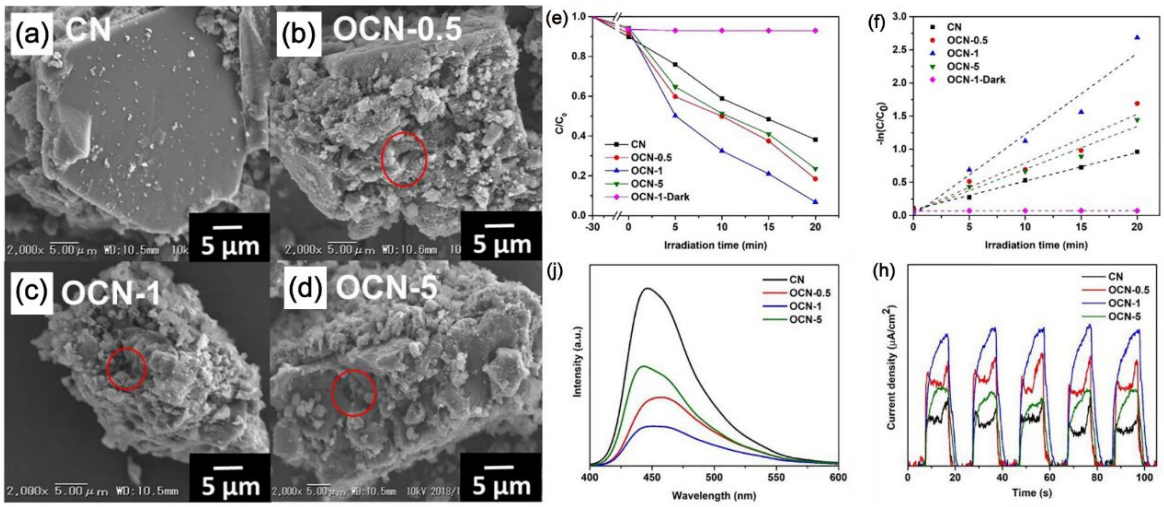

Figure 21. SEM images of (**a**) CN, (**b**) OCN-0.5, (**c**) OCN-1, and (**d**) OCN-5 of SEM images; (**e**) course and (**f**) pseudo-first-order kinetics plots of photocatalytic degradation of CIP over CN and OCN samples; (**g**) PL spectra, (**h**) photocurrent response, spectra of pure CN, OCN-0.5, OCN-1, and OCN-5. Figures taken with permission from reference [133].

Recently, the introduction of carbon quantum dots (CQDs) into PCN has received growing attention. Balakumar et al. [134] CQDs and polyaniline (PANI) to the g-C_3N_4 to form CN-Pani-CQDs photocatalyst by *in-situ* polymerization and ultrasonic treatment. The optimized CQDs loaded CN-PANI nanocomposites have higher specific surface area and higher visible light absorption. Ultrasonic technology is also an effective method for porous formation. Wang et al. [135] reported a novel photocatalyst with zero-dimensional CQDs implanted in one-dimensional porous tubular g-C_3N_4 on carbon cloth (CC). g-C_3N_4 nanotubes were synthesized on CC by using a zinc oxide sacrificial template, and g-C_3N_4/CQD microregion heterojunction photocatalyst (g-C_3N_4/CQD/CC) was constructed. The degradation of CIP reached 98% within 60 min under visible light irradiation and the degradation rate reached 0.1137 min^{-1}. CQDs can strongly interact with g-C_3N_4 and provide more active sites, degrade toxic chemicals, and have good stability. However, there are still not many reports on this aspect, and it is worth exploring deeply.

The construction of heterojunction will reduce the recombination rate of photogenerated charge, which is also a powerful measure to improve the photocatalytic efficiency of materials. Li et al. [136] designed a new S-scheme photocatalyst g-C_3N_4/C-TiO_2 by one-step calcination and gas-template method. G-C_3N_4 is separated into

a porous sheet structure, the formation of S-type heterojunction and large specific surface area, up to 90.4832 m^2/g (Figure 22a,b), and the separation efficiency and transferability of photogenerated carrier are significantly improved (Figure 22c,d). The degradation rate of 0.5%-TCN-2 was 8.9 times higher than that of pure CN within 50 min (Figure 22e,f). This work provides an idea for the synthesis of other novel photocatalysts. Qin et al. [137] synthesized g-C_3N_4/MIL-101(Fe) heterojunction hybrid by simple solvothermal method. By constructing heterojunction at the interface, visible light utilization and carrier separation are enhanced, and the electrocatalytic capability is improved. Within 240 min, the decomposition rate of antibiotics reached 87.55%. Metal-organic frames (MOF) have become a new type of material due to their porous structure, open metal location and customizable chemical properties. It has a good application prospect to synthesize new PCN composite with carbon nitride through morphology regulation.

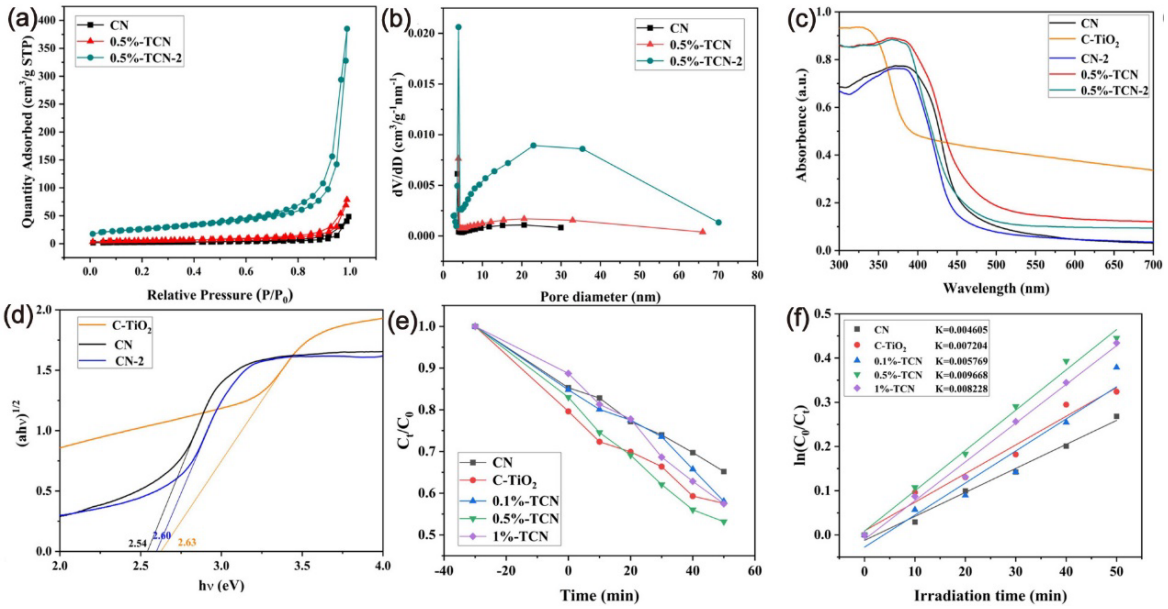

Figure 22. N_2 adsorption-desorption isotherms (**a**) and the corresponding pore size distribution curves (**b**) of CN, 0.5%-TCN, 0.5%-TCN-2; (**c**) UV-Vis spectra of CN, C-TiO_2, CN-2, 0.5%-TCN, 0.5%-TCN-2 and (**d**) the tauc plots of CN, CN-2, C-TiO_2; (**e**) Degradation of CIP · HCl by as-prepared samples; (**f**) the kinetic behavior of CIP · HCl degradation over as-prepared samples. Figures taken with permission from reference [136].

4.3. Norfloxacin Degradation

In recent years, the problem of environmental pollution caused by drugs and personal care products has become increasingly prominent. Norfloxacin (NOR), as a representative fluoroquinolone antibiotic, has been widely used in clinical treatment. Unfortunately, most NOR is prone to release into the environment, with potential adverse effects on human health and ecosystems. g-C_3N_4 has been a research hotspot in the field of environmental pollution control due to its remarkable response to visible light (approximately 450–460 nm), dependable chemical properties, excellent thermal stability and adaptable electronic structure. However, the inherent defects of g-C_3N_4 such as low specific surface area, and rapid electron-hole recombination severely limit its practical application in photocatalysis. In order to overcome these shortcomings, various methods have been used to improve its photocatalytic activity, including element doping, heterojunction modification, morphological control and coupling with narrow band gap semiconductor materials. This section focuses on the application of PCN for the degradation of NOR.

Heteroatom doping is an attractive strategy to regulate the electronic structure of semiconductors and improve their photocatalytic performance. Yang et al. [138] successfully synthesized P and Cl co-doped with nitrogen deficient g-C_3N_4 (G-Cl/g-C_3N_4) by using ammonium phosphate and ammonium chloride as doping agents and melamine thermal shrinkage method. The addition of P and Cl atoms to the g-C_3N_4 unit greatly changed the chemical properties of g-C_3N_4. NH_4Cl atmosphere promoted the formation of nanosheets, produced nitrogen defects, increased the specific surface area, and inhibited the electron-hole pair recombination. The possible degradation mechanism was explained as follows (Figure 23):

$$\text{ClPCN-2} + h\nu \rightarrow \text{ClPCN-2}\ (e^- + h^+) \quad (1)$$

$$O_2 + e^-/\text{defects} \rightarrow \bullet O_2^- \quad (2)$$

$$h^+/\bullet O_2^- + \text{RHB/NOR} \rightarrow \text{degradation products} \quad (3)$$

The photocatalytic performance of the prepared P and Cl co-doped g-C_3N_4 for the NOR degradation was significantly improved, which was 2.0 times than that of the original g-C_3N_4 and the degradation rate reached 0.047 min^{-1}. This work provides a simple and effective method for constructing doped g-C_3N_4 materials with nonmetallic elements and defective structures.

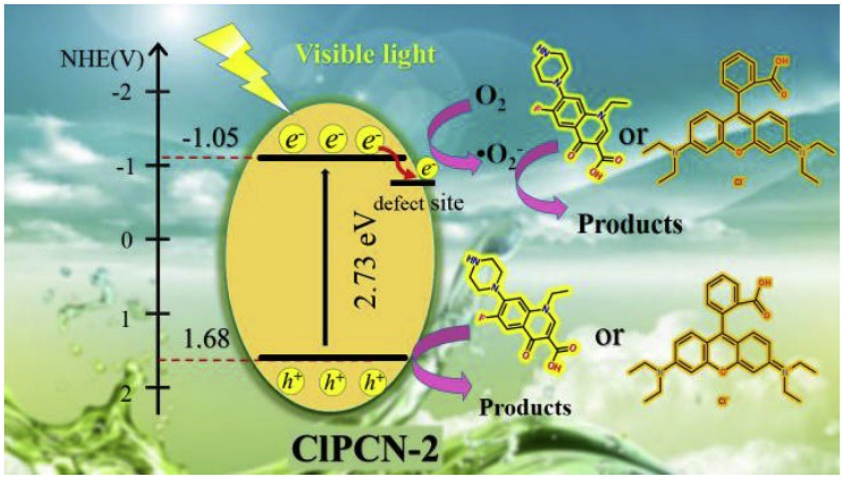

Figure 23. Photocatalytic mechanism scheme of ClPCN-2 sample under visible light irradiation. Figures taken with permission from reference [138].

Ding et al. [139] reasonably designed and synthesized N-doped g-C_3N_4 (CoFe@N-GC) coated CoFe alloy particles which were converted from cobalt-modified Prussian blue (PB) precursor by two-step carbonization in situ. The resulting hybrid catalyst could not only provide a conductive network to promote electron transfer, but also protect the metal species from leaching.

In order to achieve full spectrum absorption and maximum electron-hole pair separation, the self-modification strategy provides a reasonable and interesting method for the preparation of efficient PCN photocatalysts. Li et al. [140] successfully prepared a novel ternary photocatalyst Ag/CNQDs/g-C_3N_4 composite by microwave-assisted process combined with chemical reduction method (Figure 24a). The synergistic effect of up conversion characteristics of CNQDs and SPR effect of Ag nanoparticles can improve the charge separation efficiency (Figure 24b,c). The formation of homologous heterojunction between CNQDs and g-C_3N can generate an internal electric field. This is conducive to the efficient separation of charged carriers. As a result, NOR removal rate reached almost 100% within 120 min and the degradation rate was 0.047 min^{-1} (Figure 24d,e). This work not only provides new insights into the design of PCN composites for photocatalytic applications, but also provides an effective strategy in the field of environmental remediation.

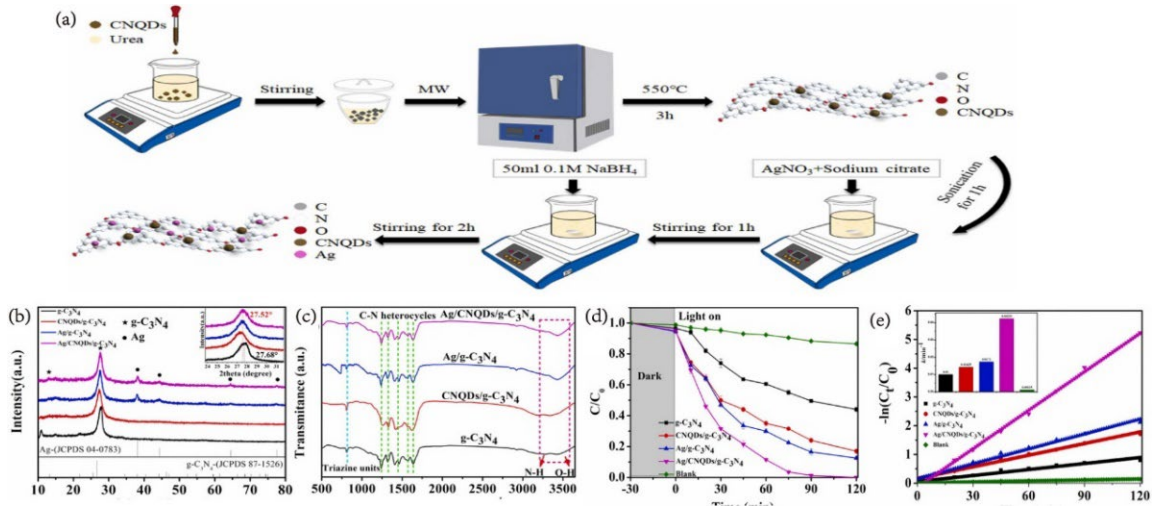

Figure 24. (**a**) The diagram for the synthesis of Ag/CNQDs/g-C_3N_4 composites; (**b**) XRD spectrum; (**c**) FT-IR spectra; (**d**) Photocatalytic degradation curves and (**e**) the corresponding pseudo-first-order reaction kinetic curves and the apparent rate constants k (insert) of the as-obtained samples. Figures taken with permission from reference [140].

4.4. Others

Antibiotic species is a large family with complicated structure and high stability. Nevertheless, antibiotics show an outstanding performance in the field of antibacterial, some troubles caused by overusing like aspirin [141], enrofloxacin [142] and chloramphenicol [143] still need to solve. This section will introduce the degradation methods of several common antibiotics. High levels of Diclofenac (DCF) can cause poisoning and population decline in fish, aquatic organisms and birds. Recently, Shojaeimehr et al. [144] investigated the photo degradation of diclofenac in a continuous flow reactor by fixing synthetic PCN particles on a stainless steel (SS) plate. The DCF removal efficiency of the material is about 71%. The reaction rate constant is 0.0049 min^{-1}. Compared with the degradation of DCF by suspended photocatalyst particles reported in other literatures, the continuous flow reactor has more practical application value, which provides a feasible idea for the development of photocatalyst. On the other hand, the combination of defect engineering and morphology control is also an effective strategy to enhance photocatalytic degradation of antibiotics. Zhong et al. [145] synthesized PCN with Na doping and N defect by thermal polymerization. Skeleton structure is shown in Figure 25a. The optimized carbon nitride provides the endogenous power for the directional separation of the disordered carrier. At the same time, bridging Na can be used as the adsorption site of Fluoroquinolone (FLP) antibiotics. After optimization, the degradation rate of the sample to FLP can reach 0.5932 min^{-1}, which is 11 times that of the original carbon nitride. The concept of disordered charge directed utilization can also be referenced to other catalysts, thus guiding the development of new catalysts. Li et al. [146] synthesized N-rich porous carbon nitride rich in amino defects by hot polymerization (Figure 25b). The highly fractional cyanic acid in the polymer intermediate acts as a pore agent to provide a porous structure for the reaction. The removal rate of levofloxacin (LEV, 50 mg L^{-1}) reached 93.5% within 60 min (Figure 25c) which more than most photocatalysts reported to date. Amino defect engineering provides a good strategy for PCN modification. Enhancing the specific surface area is an effective method to modify carbon nitride. Ding et al. [147] synthesized g-C_3N_4 composite material with hollow tube structure through a new molten salt-assisted thermal condensation strategy. Molten salt assisted thermal condensation transforms g-C_3N_4 from massive to hollow tubular, which provides a platform for the loading of biomass porous carbon (BPC). BPC loaded with g-C_3N_4 can be used as the active site to improve the removal efficiency of oxytetracycin (OTC) by adsorption. The photocatalytic degradation efficiency of oxytetracycline OTC in the best samples was up to 84% (Figure 25d,e). It can be seen that the strategy of introducing porous activated carbon with large specific surface area and strong adsorption capacity to synthesize composite photocatalyst, and then produce the synergistic effect of adsorption and photo degradation, and enhance the photocatalytic performance is worthy of further study. Forming tubular structure is a method to enhance the photocatalytic performance of porous carbon nitride. Lei at al. [135] recently prepared ultra-thin black phosphorus quantum dots (BPQDs) loaded carbon nitride nanohybrid materials with one-dimensional tubular structure by ultrasonic method and high vacuum stirring method. The morphology of different samples is shown in the Figure 25f–h, and the obvious tubular structure of composite samples can be seen. The combination of tubular g-C_3N_4 with BPQDs contributes to the separation of charge space during photocatalysis. It is specially designed 0D/1D structure shows high photocatalytic activity for the degradation of Oxytetricin(OTL) hydrochloride (0.0276 min^{-1}). This study provides a broad prospect for metal-free nanomaterials with high photocatalytic properties.

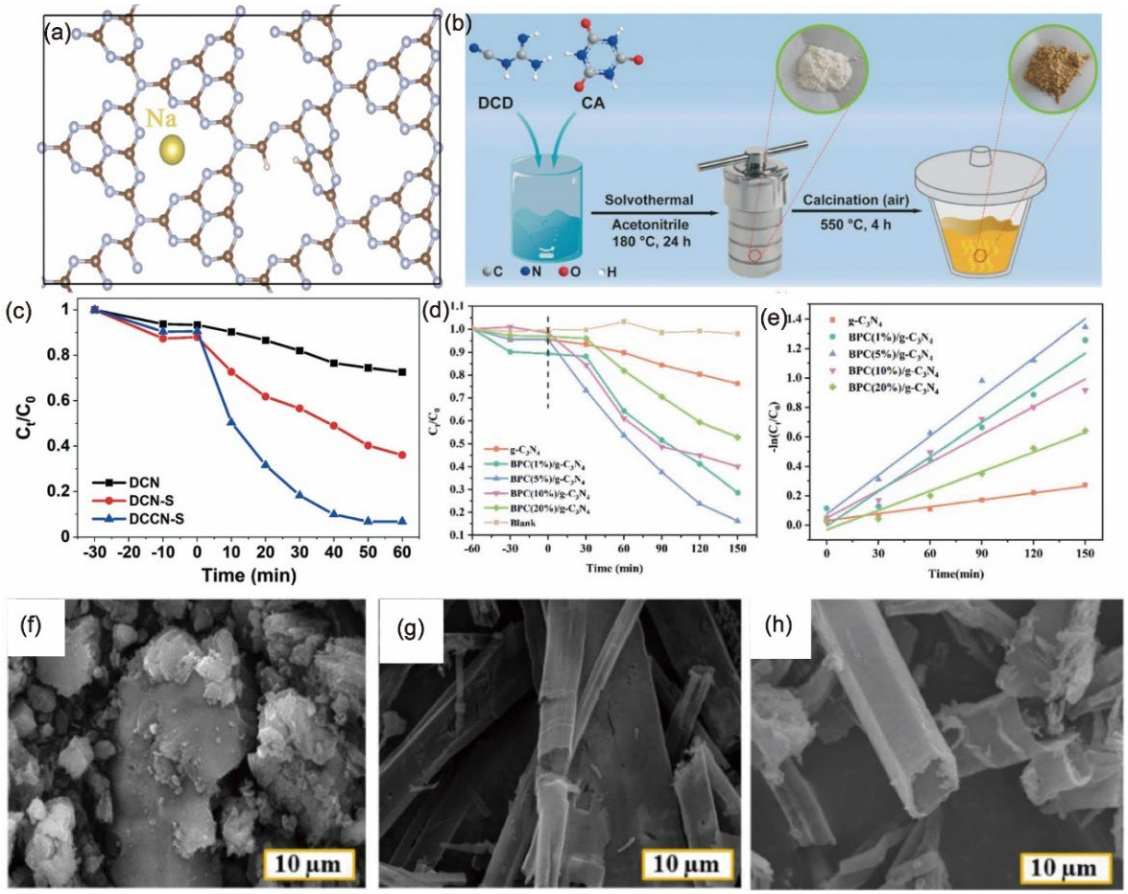

Figure 25. (**a**) proposed framework structure of 8WNCN, (Brown atoms: C atoms, silver atoms: N atoms, yellow atom: Na atoms); (**b**) Schematic illustration for the preparation of DCCN-S; (**c**) Removal rates of LEV over different photocatalysts; (**d**) Photocatalytic degradation of OTC on the g-C_3N_4 and BPC(X%)/ g-C_3N_4 composites under visible light illumination; (**e**) the first-order kinetics curve of the g-C_3N_4 and BPC(X%)/g-C_3N_4 composites for OTC photo degradation; Microscopic characterization of obtained samples. SEM images of (**f**) CN; (**g**) TCN; and (**h**) BPTCN, respectively. Figures taken with permission from reference [133–136].

Herein, we summary various parameters for the degradation of antibiotics over different PCN photocatalysts as shown in Table 1. Most PCN photocatalysts currently used to degrade TC display highly efficient photocatalytic performance, and the optimal degradation efficiency can reach about 100% within 60 min. By comparing the first order kinetic reaction constant K. It is not difficult to find that the photocatalyst prepared by Chuaicham et al. [148] has a high reaction rate of 0.2600 min^{-1}. The composite material's interface may shrink and form an electron trap state due to its ingenious design. This traps the excited electrons and prevents charge recombination, increasing the electrons' and holes' separation ability. Therefore, it is a feasible way to find new semiconductor materials and g-C_3N_4 composite to form heterojunction and enhance photocatalytic degradation of antibiotics. The reaction rate of the composite prepared by Zhong et al. [145] reached 0.5932 min^{-1}, which exceeded that of most reported G-based catalysts. The possible reason is that it is easy to overlook the potential of g-C_3N_4 as a Lewis base adsorption site when studying the regulation of the electrical conductivity of the structure. In this paper, the combination of defect engineering and Na doping was used to improve the carrier concentration and the directional utilization of internal carriers, and optimize the redox activity. The PCN composite prepared by Preeyanghaa et al. [121] can degrade nearly 100 percent of TC within 60 min. Its novel sound-photocatalysis strategy, which combines ultrasound and photocatalysis and provides a new idea of antibiotic degradation. The ternary heterojunction PCN composite photocatalyst constructed by Li et al. [140] by microwave assisted method also showed a good degradation effect on NOR (~100%/120 min^{-1}), indicating that it is feasible to construct S-type heterojunction and form an internal electric field to improve the photodegradation of antibiotics. In summary, it can be found that it is difficult to greatly break through the original degradation efficiency of g-C_3N_4-photocatalyst by adopting a single strategy. However, it has a broad prospect to construct PCN composites by the combination of morphology control, defect engineering and heterogeneous structure construction. At the same time, there are still not many reports on this area, and more in-depth exploration is needed. In addition, due to the limited use of light, low

photocatalytic efficiency, photocatalyst preparation conditions and other factors, it is difficult to achieve large-scale degradation experiments, which is also the factors that need to be considered in our later experiments.

Table 1. Comparison of the photocatalytic antibiotic degradation performance over porous g-C_3N_4-based photocatalysts.

Photocatalysts	Conditions (Wavelength, Photocatalyst, Antibiotic, Concentration)	Antibiotic Molecules	Degradation Efficiency/Time	K_{app} [a] (min^{-1})	Ref
Cu-PCN	Xl 300 W; >420 nm; 30 mg; 30 mg/L	TC	98%/120	-	[116]
B-PCN	Xl 300 W; >420 nm; 10 mg; 40 mg/L	TC	81.3%/120	-	[117]
N-GQDs/P-g-C_3N_4	Xl 500 W; >420 nm; 10 mg; 20 mg/L	TC	89.9%/60	0.0313	[118]
C/O/g-C_3N_4	Xl 300 W; >420 nm; 20 mg; 20 mg/ L	TC	89%/60	0.0908	[120]
Cv-g-C_3N_4	Xl 300 W; >420 nm; 10 mg; 15 mg/L	TC	100 %/60	-	[121]
Nv-g-C_3N_4	LED 50 W; - ; 50 mg; 20 mg/L	TC	78 %/120	0.0100	[122]
CN/CNT/BWO	Wl 500 W; - ; 40 mg; 35 mg/L	TC	87.65%/90	-	[123]
ZnO/g-C_3N_4	Xl 300 W; >400 nm; 20 mg; 20 mg /L	TC	78.4%/50	-	[124]
2D/2D-SCN	Xe 300 W; >420 nm; 20 mg; 20 mg/L	TC	82.2%/60	0.0279	[125]
OCN	Xl 500 W; >380 nm; 50 mg; 10 mg/L	CIP	95%/20	0.1220	[133]
CN-PANI/CQDs	Xl 500 W; >420 nm; 50 mg; 10 mg /L	CIP	87.6%/90	-	[134]
g-C_3N_4/CQD/CC	Xl 250 W; >420 nm; 40 mg; 5 mg/L	CIP	98%/60	0.1137	[135]
g-C_3N_4/C-TiO_2	Xl 300 W; >420 nm; 30 mg; 20 mg/L	CIP	88.14%/50	-	[136]
g-C_3N_4/MIL-101(Fe)	LED 12 W; >420 nm; 50 mg; 10 mg/L	CIP	92.99%/250	0.0090	[137]
CN/ZnTi-MMO	Xe 500W; >380 nm; 50 mg;10 mg/L	CIP	100%/20	0.2600	[148]
P-Cl/g-C_3N_4	LED 70 W; >420 nm; 50 mg; 10 mg/L	NOR	99.62%/120	0.0470	[138]
Ag/CNQDs/g-C_3N_4	visible light; >420 nm; 10 mg; 10 mg/L	NOR	100%/120	0.0423	[140]
CQD-CNs/BWO	Xl 500 W; >420 nm; 50 mg; 15 mg/L	NOR	67.6%/120	0.0078	[149]
PCN/(001)-TiO_2	Xe 300 W; UV–vis light; 50 mg; 10 mg/L	NOR	99%/90	0.0299	[150]
MP-CN	Xl 300 W; >420 nm; 25 mg; 10 mg/L	DCF	71%/120	0.0049	[144]
WNCN	LED 9 W; - ; 20 mg ; 10 mg/L	CLP	-	0.5932	[145]
DCCN-S	Xl 300 W; >420 nm; 25 mg; 50 mg/L	LEV	93.5%/60	0.0500	[146]
BPC	Xl 300 W; >420 nm; 50 mg; 10 mg/L	OTC	84%/120	0.0088	[147]
BPTCN	Xl 300 W; >420 nm; 30 mg; 10 mg /L	OTL	81.05%/60	0.0276	[151]

[a] K_{app} represents the reaction rate constant.

5. Challenges and Perspectives

Photocatalytic technology is an effectively approach to solve the issues of antibiotic pollution in water system due to the direct utilization of solar energy. Then, PCN is also considered a promising photocatalytic material for antibiotic degradation, which is mainly attributed to the simple synthesis, low-cost, non-pollution and non-toxicity. In addition, porous, rapid electrons migration and abundant active sites are benefit to PCN material for photocatalytic antibiotic degradation. However, the bottleneck still exists in using monomer PCN for photocatalytic reaction, such as, photogenerated carriers have insufficient kinetics to support active radicals and fast photogenerated carrier recombination. Thus, substantial works have been done to improve the catalytic active for antibiotic degradation.

The template method can efficiently prepare PCN with a high specific surface area. However, the use of hard templates in the preparation process usually requires toxic template removers, while. soft templates release toxic gases during the formation process. Although supramolecular self-assembly can avoid toxic removal agents and harmful gases, the preparation of supramolecular precursors requires the use of organic reagents. Therefore, determining the hard and soft templates that are pollution free, easy to operate and cost effective is a top priority for future work.

The alteration in morphology is favourable for improving the photocatalytic performance of PCN. One-dimensional nanorods, nanotubes, and nanowires' electron confinement effect can suppress electron hole recombination. However, the synthesis methods typically require templates and crystallization, resulting in cumbersome operation steps, high energy consumption, and pollution problems. Although 2D nanosheets have high specific surface areas and favourable optical properties, the potential disadvantages of their synthesis need to be considered. For example, it produces a lot of harmful gases. The three-dimensional structure exhibits effective adsorption properties for pollutants, but there are still few reports on its application at present.

Defect engineering is a promising strategy for improving optical response and catalytic performance. However, the presence of defects may affect the crystalline structure of g-C3N4. Therefore, determining the ideal number of defects or vacancies is a prerequisite for effectively collecting photo-generated electrons, separating them from holes, and improving photocatalytic performance.

Element doping is a common strategy to enhance photocatalytic activity through metal doping, non-metal doping, co-doping and heterojunctions based on doped g-C3N4. By modulating the orientation of HOMO and LUMO, both have catalytic oxidation-reduction potentials, while reducing their bandgap and broadening the photoresponse range of g-C3N4. Enhance the separation of photo generated electrons and holes. However, the thermal stability of doped ions is often limited. Furthermore, the newly generated energy bands may act as recombination centres, resulting in a reduction in quantum efficiency. Co-doping or triple doping could be a viable strategy that combines the benefits of these individual doping methods to positively impact the structure and optical properties.

PCN is a promising material applied in the field of photocatalytic antibiotic degradation. However, there are challenges associated with PCN photocatalytic antibiotic degradation as shown below:

(i) Antibiotic complexity: Antibiotics have diverse chemical structures, and their degradation pathways can vary. Understanding the specific degradation mechanisms for different antibiotics is crucial for optimizing the photocatalytic process.

(ii) Reaction conditions optimization: The photocatalytic degradation efficiency of PCN can be influenced by factors such as light intensity, reaction temperature, pH, and catalyst loading. Finding the optimal reaction conditions for each antibiotic is essential to maximize degradation efficiency.

(iii) Degradation intermediates and byproducts: During the photocatalytic degradation process, intermediate products or byproducts may form, some of which could be potentially harmful. Identifying and minimizing the formation of these byproducts is important to ensure environmental safety.

To address these challenges and further advance the field of PCN photocatalytic antibiotic degradation, future research can focus on the following aspects:

(i) Material design and synthesis: Developing novel PCN materials with enhanced photocatalytic properties, such as improved surface area and enhanced light absorption, to achieve higher degradation efficiency.

(ii) Mechanism investigation: Investigating the degradation mechanisms of different antibiotics on PCN surfaces to understand the underlying pathways and intermediates involved in the degradation process.

(iii) Process optimization: Experimentally optimizing the reaction conditions, including light intensity, temperature, pH, and catalyst loading, to achieve maximum degradation efficiency for different antibiotics.

(iv) Toxicity assessment: Conducting comprehensive toxicity assessments of the degradation products and byproducts generated during the photocatalytic process to ensure the safety of the environment and human health.

6. Conclusions and Outlook

Photocatalytic technology is an effectively approach to solve the issues of antibiotic pollution in water system due to the direct utilization of renewable solar energy. In addition, PCN is also considered to be promising photocatalytic material for antibiotic degradation, which is mainly attributed to their simple synthesis, low-cost, non-pollution and non-toxicity natures. Moreover, porous, rapid electrons migration, and abundant active sites are benefit to PCN material for photocatalytic antibiotic degradation. However, the bottleneck still exists in using single PCN for photocatalytic reaction such as photogenerated carriers have insufficient kinetics to support active radicals and fast photogenerated carrier recombination. Thus, substantial works have been done to improve the catalytic activity. In this review, we have summarized the synthesis strategies for PCN in terms of bottom-up and top-down approach. Then, the structure engineering of PCN is illustrated from the aspect of morphological structures, functional structure, and hybridization. Subsequently, the application in the field of photocatalytic antibiotic degradation over PNC has been discussed. PCN possesses a large surface area and unique pore structure, which enhances its photocatalytic activity and provides an effective platform for antibiotic degradation. In summary, the PCN-based photocatalysts for antibiotic degradation is promising, with several advantages as below:

(i) Enhanced photocatalytic activity: The porous structure of PCN increases the surface area available for catalytic reactions, leading to improved photocatalytic efficiency in degrading antibiotics.

(ii) Applicability for various antibiotics: PCN-based photocatalysts exhibit excellent degradation capabilities for a wide range of antibiotics, making it applicable to various pollutants.

(iii) Stability and reusability: PCN-based photocatalysts are stable under photocatalytic conditions and can be easily recovered and reused, reducing material consumption and cost.

(iv) Environmental friendliness: Compared to traditional methods, PCN-based photocatalysts requires only light energy and does not generate harmful byproducts, making it environmentally friendly.

Additionally, some bottlenecks still need to be taken seriously as bellow:

(i) Although many active sites made of low-coordinated atoms can be produced in defect sites by the highly structured mesopores and unique structure of PCN-based photocatalysts, the corresponding green synthesis techniques are still in their infancy. Doping heteroatoms in particular may have an impact on PCN-based photocatalyst shape in order to improve catalytic performance even more. As a result, researching various modification strategies is also required.

(ii) The direction of future progress is the study of theoretical computations. By using molecular simulations and reaction kinetics, theoretical calculations can explain electronic band structures and reaction mechanisms. This knowledge can be used to inform catalyst design and modification. PCN-based photocatalyst theoretical calculations are still in their infancy and are fraught with difficulties.

(iii) The other uses, such building membrane systems and controlling leachate, are still in their infancy. Because leachate control is tied to daily living, developing effective technologies is essential. Building membrane systems makes it easy to recycle samples and combine them with other physical or biological technologies for increased degradation. Additionally, more research on the pertinent applications is required.

(iv) An analysis of the potential effects on the environment is also required. The poisoning of hybridized PCN-based photocatalysts still need further investigation, notwithstanding the low cytotoxicity of PCN-based photocatalysts. In addition, it's important to talk about the toxicity studies of intermediates in the degradation process to minimize any dangers.

In conclusion, PCN-based photocatalysts for antibiotic degradation shows great potential as an effective and environmentally friendly approach. However, further research and development are evidently needed to overcome the existing challenges and optimize its performance for various antibiotics. Therefore, in the developing fields of PCN for antibiotic degradation, there is a growing potential and room for advancement for scholarly findings to be promptly applied to new technologies.

Author Contributions: Writing—original draft preparation, conceptualization, methodology, software, Z.W. and G.D.; data curation, visualization, investigation, J.Z., P.W., and Q.L.; visualization, investigation, Y.N.; supervision, software, validation, writing—reviewing and editing, funding, G.L. All authors have read and agreed to the published version of the manuscript.

Funding: This work was supported by the National Natural Science Foundation of China (Grant No. 52203110) and the Knowledge Innovation Program of Wuhan-Shuguang Project (Grant No. 2022010801020216).

Conflicts of interest: There are no conflict of interest to declare.

References

1. Qiao, Y.; Sun, C.; Jian, J.; Zhou, T.; Xue, X.; Shi, J.; Che, G.; Liao, G. Efficient removal of organic pollution via photocatalytic degradation over a TiO_2@HKUST-1 yolk-shell nanoreactor. *J. Mol. Liquids* **2023**, *385*, 122383.
2. Wu, Q.; Wang, J.; Wang, Z.; Xu, Y.; Xing, Z.; Zhang, X.; Guan, Y.; Liao, G.; Li, X. High-loaded single Cu atoms decorated on N-doped graphene for boosting Fenton-like catalysis under neutral pH. *J. Mater. Chem. A* **2020**, *8*, 13685–13693.
3. Liu, S.; Deng, F.; Guo, Y.; Ouyang, C.; Yi, S.; Li, C.; Liao, G.; Li, Q. Silver Nanocatalysts Supported by Multiple Melanin Carriers with a Photothermal Effect for Reduction of Methylene Blue and 4-Nitrophenol. *ACS Appl. Nano Mater.* **2024**, *7*, 889–903.
4. Liu, S.; Guo, Y.; Yi, S.; Yan, S.; Ouyang, C.; Deng, F.; Li, C.; Liao, G.; Li, Q. Facile synthesis of pure silicon zeolite-confined silver nanoparticles and their catalytic activity for the reduction of 4-nitrophenol and methylene blue. *Sep. Purif. Technol.* **2023**, *307*, 122727.
5. Zandieh, M.; Griffiths, E.; Waldie, A.; Li, S.; Honek, J.; Rezanezhad, F.; Van Cappellen, P.; Liu, J. Catalytic and biocatalytic degradation of microplastics. *Exploration* **2023**, p. 20230018. https://doi.org/10.1002/EXP.20230018.
6. Ding, G.; Li, C.; Ni, Y.; Chen, L.; Shuai, L.; Liao, G. Layered double hydroxides and their composites as high-

performance photocatalysts for CO_2 reduction. *EES Catal.* **2023**, *1*, 369–391.
7. Du, C.; Xu, J.; Ding, G.; He, D.; Zhang, H.; Qiu, W.; Li, C.; Liao, G. Recent Advances in LDH/g-C_3N_4 Heterojunction Photocatalysts for Organic Pollutant Removal. *Nanomaterials* **2023**, *13*, 3066.
8. Cao, W.; Zhang, W.; Dong, L.; Ma, Z.; Xu, J.; Gu, X.; Chen, Z. Progress on quantum dot photocatalysts for biomass valorization. *Exploration* **2023,** *3*, 20220169.
9. Liao, G.; Li, Q.; Zhao, W.; Pang, Q.; Gao, H.; Xu, Z. In-situ construction of novel silver nanoparticle decorated polymeric spheres as highly active and stable catalysts for reduction of methylene blue dye. *Appl. Catal. A Gen.* **2018**, *549*, 102–111.
10. Liao, G.; Gong, Y.; Zhong, L.; Fang, J.; Zhang, L.; Xu, Z.; Gao, H.; Fang, B. Unlocking the door to highly efficient Ag-based nanoparticles catalysts for $NaBH_4$-assisted nitrophenol reduction. *Nano Res.* **2019**, *12*, 2407–2436.
11. Tahir, M.; Tahir, B. In-situ growth of TiO_2 imbedded $Ti_3C_2T_A$ nanosheets to construct PCN/$Ti_3C_2T_A$ MXenes 2D/3D heterojunction for efficient solar driven photocatalytic CO_2 reduction towards CO and CH_4 production. *J. Colloid Interface Sci.* **2021**, *591*, 20–37.
12. Liu, C.; Tan, L.; Zhang, L.; Tian, W.; Ma, L. A Review of the Distribution of Antibiotics in Water in Different Regions of China and Current Antibiotic Degradation Pathways. *Front. Environ. Sci.* **2021**, *9*, 692298.
13. Zheng, G.; He, J.; Kumar, V.; Wang, S.; Pastoriza-Santos, I.; Pérez-Juste, J.; Liz-Marzán, L. M.; Wong, K.-Y. Discrete metal nanoparticles with plasmonic chirality. *Chem. Soc. Rev.* **2021**, *50*, 3738–3754.
14. Liao, G.; Ding, G.; Yang, B.; Li, C. Challenges in Photocatalytic Carbon Dioxide Reduction. *Precis. Chem.* **2024**. https://doi.org/10.1021/prechem.3c00112.
15. Liao, G.; He, Y.; Wang, H.; Fang, B.; Tsubaki, N.; Li, C. Carbon neutrality enabled by structure-tailored zeolite-based nanomaterials. *Device* **2023**, *1*, 100173.
16. Suyana, P.; Ganguly, P.; Nair, B.N.; Pillai, S.C.; Hareesh, U. S. Structural and compositional tuning in g-C_3N_4 based systems for photocatalytic antibiotic degradation. *Chem. Eng. J. Adv.* **2021**, *8*, 100148.
17. Zhang, J.; Shen, B.; Hu, Z.; Zhen, M.; Guo, S.Q.; Dong, F. Uncovering the synergy between Mn substitution and O vacancy in ZnAl-LDH photocatalyst for efficient toluene removal. *Appl. Catal. B Environ.* **2021**, *296*, 120376.
18. Zhou, J.; Shan, T.; Zhang, F.; Boury, B.; Huang, L.; Yang, Y.; Liao, G.; Xiao, H.; Chen, L. A Novel Dual-Channel Carbon Nitride Homojunction with Nanofibrous Carbon for Significantly Boosting Photocatalytic Hydrogen Peroxide Production. *Adv. Fiber Mater.* **2024**. https://doi.org/10.1007/s42765-023-00354-9.
19. Wang, Z.; Ding, G.; Zhang, J.; Lv, X.; Wang, P.; Shuai, L.; Li, C.; Ni, Y.; Liao, G. Critical role of hydrogen bonding between microcrystalline cellulose and g-C_3N_4 enables highly efficient photocatalysis. *Chem. Commun.* **2024**, *60*, 204–207.
20. Shan, T.; Li, J.; Wu, S.; Wu, H.; Zhang, F.; Liao, G.; Xiao, H.; Huang, L.; Chen, L. Boosting H_2O_2 production over carboxymethyl cellulose modified g-C_3N_4 via hydrogen-bonding-assisted charge transfer. *Chem. Eng. J.* **2023**, *478*, 147509.
21. Liao, G.; Gong, Y.; Zhang, L.; Gao, H.; Yang, G.-J.; Fang, B. Semiconductor polymeric graphitic carbon nitride photocatalysts: the “holy grail” for the photocatalytic hydrogen evolution reaction under visible light. *Energy Environ. Sci.* **2019,** *12*, 2080-2147.
22. Xue, J.; Ma, S.; Zhou, Y.; Zhang, Z.; He, M. Facile Photochemical Synthesis of Au/Pt/g-C_3N_4 with Plasmon-Enhanced Photocatalytic Activity for Antibiotic Degradation. *ACS Appl. Mater. Interfaces* **2015**, *7*, 9630–9637.
23. Xiao, M.; Luo, B.; Wang, S.; Wang, L. Solar energy conversion on g-C_3N_4 photocatalyst: Light harvesting, charge separation, and surface kinetics. *J. Energy Chem.* **2018**, *27*, 1111–1123.
24. Minshull, T. C.; Cole, J.; Dockrell, D. H.; Read, R. C.; Dickman, M. J. Analysis of histone post translational modifications in primary monocyte derived macrophages using reverse phasexreverse phase chromatography in conjunction with porous graphitic carbon stationary phase. *J. Chromatogr. A* **2016**, *1453*, 43–53.
25. Xiao, Y.; Tian, G.; Li, W.; Xie, Y.; Jiang, B.; Tian, C.; Zhao, D.; Fu, H. Molecule Self-Assembly Synthesis of Porous Few-Layer Carbon Nitride for Highly Efficient Photoredox Catalysis. *J. Am. Chem. Soc.* **2019**, *141*, 2508–2515.
26. Zhao, Y.; Law, H.C.; Zhang, Z.; Lam, H.C.; Quan, Q.; Li, G.; Chu, I.K. Online coupling of hydrophilic interaction/strong cation exchange/reversed-phase liquid chromatography with porous graphitic carbon liquid chromatography for simultaneous proteomics and N-glycomics analysis. *J. Chromatogr. A* **2015**, *1415*, 57–66.
27. Liu, Q.; Chen, C.; Yuan, K.; Sewell, C. D.; Zhang, Z.; Fang, X.; Lin, Z. Robust route to highly porous graphitic carbon nitride microtubes with preferred adsorption ability via rational design of one-dimension supramolecular precursors for efficient photocatalytic CO_2 conversion. *Nano Energy* **2020**, *77*, 105104.
28. Wang, J.; Wang, S. A critical review on graphitic carbon nitride (g-C_3N_4)-based materials: Preparation, modification and environmental application. *Coordin. Chem. Rev.* **2022**, *453*, 214338.
29. Estevez, L.; Prabhakaran, V.; Garcia, A.L.; Shin, Y.; Tao, J.; Schwarz, A.M.; Darsell, J.; Bhattacharya, P.; Shutthanandan, V.; Zhang, J.G. Hierarchically Porous Graphitic Carbon with Simultaneously High Surface Area and Colossal Pore Volume Engineered via Ice Templating. *ACS Nano* **2017**, *11*, 11047–11055.
30. Brezesinski, T.; Groenewolt, M.; Antonietti, M.; Smarsly, B. Crystal-to-Crystal Phase Transition in Self-Assembled Mesoporous Iron Oxide Films. *Angew. Chem. Int. Ed.* **2006**, *45*, 781–784.
31. Peer, M.; Lusardi, M.; Jensen, K.F. Facile Soft-Templated Synthesis of High-Surface Area and Highly Porous Carbon Nitrides. *Chem. Mater.* **2017**, *29*, 1496–1506.

32. Yang, Z.; Zhang, Y.; Schnepp, Z. Soft and hard templating of graphitic carbon nitride. *J. Mater. Chem. A* **2015**, *3*, 14081–14092.
33. Zhou, Y.; Wu, Y.; Wu, H.; Xue, J.; Ding, L.; Wang, R.; Wang, H. Fast hydrogen purification through graphitic carbon nitride nanosheet membranes. *Nat. Commun.* **2022**, *13*, 5852.
34. Obregón, S.; Vázquez, A.; Ruíz-Gómez, M.A.; Rodríguez-González, V. SBA-15 assisted preparation of mesoporous g-C_3N_4 for photocatalytic H_2 production and Au^{3+} fluorescence sensing. *Appl. Surf. Sci.* **2019**, *488*, 205–212.
35. Lee, Y.-G.; Ahn, H.-J. Tri(Fe/N/F)-doped mesoporous carbons as efficient electrocatalysts for the oxygen reduction reaction. *Appl. Surf. Sci.* **2019**, *487*, 389–397.
36. Gibot, P.; Schnell, F.; Spitzer, D. Enhancement of the graphitic carbon nitride surface properties from calcium salts as templates. *Micropor. Mesopor. Mater.* **2016**, *219*, 42–47.
37. Tian, Z.; Yang, X.; Chen, Y.; Huang, H.; Hu, J.; Wen, B. Fabrication of alveolate g-C_3N_4 with nitrogen vacancies via cobalt introduction for efficient photocatalytic hydrogen evolution. *Int. J. Hydrogen Energy* **2020**, *45*, 24792–24806.
38. Ma, L.; Wang, G.; Jiang, C.; Bao, H.; Xu, Q. Synthesis of core-shell TiO_2 @g-C_3N_4 hollow microspheres for efficient photocatalytic degradation of rhodamine B under visible light. *Appl. Surf. Sci.* **2018**, *430*, 263–272.
39. Chen, D.; Yang, J.; Ding, H. Synthesis of nanoporous carbon nitride using calcium carbonate as templates with enhanced visible-light photocatalytic activity. *Appl. Surf. Sci.* **2017**, *391*, 384–391.
40. Zheng, Y.; Lin, L.; Wang, B.; Wang, X. Graphitic Carbon Nitride Polymers toward Sustainable Photoredox Catalysis. *Angew. Chem. Int. Ed.* **2015**, *54*, 12868–12884.
41. Liu, C.; Zhang, Y.; Dong, F.; Du, X.; Huang, H. Easily and Synchronously Ameliorating Charge Separation and Band Energy Level in Porous g-C_3N_4 for Boosting Photooxidation and Photoreduction Ability. *J. Phys. Chem. C* **2016**, *120*, 10381–10389.
42. Wang, Y.; Wang, X.; Antonietti, M.; Zhang, Y. Facile one-pot synthesis of nanoporous carbon nitride solids by using soft templates. *ChemSusChem* **2010**, *3*, 435–439.
43. Fan, Q.; Liu, J.; Yu, Y.; Zuo, S. A template induced method to synthesize nanoporous graphitic carbon nitride with enhanced photocatalytic activity under visible light. *RSC Adv.* **2014**, *4*, 61877–61883.
44. Dolai, S.; Bhunia, S.K.; Kluson, P.; Stavarek, P.; Pittermannova, A. Solvent-Assisted Synthesis of Supramolecular-Assembled Graphitic Carbon Nitride for Visible Light Induced Hydrogen Evolution—A Review. *ChemCatChem* **2021**, *14*, 1867–3880.
45. Prins, L. J.; Reinhoudt, D.N.; Timmerman, P. Noncovalent Synthesis Using Hydrogen Bonding. *Angew. Chem. Int. Ed.* **2001**, *40*, 2382–2426.
46. Shalom, M.; Inal, S.; Fettkenhauer, C.; Neher, D.; Antonietti, M. Improving carbon nitride photocatalysis by supramolecular preorganization of monomers. *J. Am. Chem. Soc.* **2013**, *135*, 7118–7121.
47. Zhou, B.-X.; Ding, S.-S.; Zhang, B.-J.; Xu, L.; Chen, R.-S.; Luo, L.; Huang, W.-Q.; Xie, Z.; Pan, A.; Huang, G.-F. Dimensional transformation and morphological control of graphitic carbon nitride from water-based supramolecular assembly for photocatalytic hydrogen evolution: From 3D to 2D and 1D nanostructures. *Appl. Catal. B Environ.* **2019**, *254*, 321–328.
48. Zhang, H.; Wu, P.; He, J.; Jiang, W.; Liu, C. Highly dispersible graphitic carbon nitride: Synthesis and its 2-electron photocatalytic reduction activity of O_2. *J. Environ. Chem. Eng.* **2021**, *9*, 106430.
49. Liu, M.-X.; Zhang, J.-Y.; Zhang, X.-L. Application of graphite carbon nitride in the field of biomedicine: Latest progress and challenges. *Mater. Chem. Phys.* **2022**, *281*, 125925.
50. Liao, G.; He, F.; Li, Q.; Zhong, L.; Zhao, R.; Che, H.; Gao, H.; Fang, B. Emerging graphitic carbon nitride-based materials for biomedical applications. *Prog. Mater. Sci.* **2020**, *112*, 100666.
51. Liu, W.; Iwasa, N.; Fujita, S.; Koizumi, H.; Yamaguchi, M.; Shimada, T. Porous graphitic carbon nitride nanoplates obtained by a combined exfoliation strategy for enhanced visible light photocatalytic activity. *Appl. Surf. Sci.* **2020**, *499*, 143901.
52. Yang, P.; Zhao, J.; Qiao, W.; Li, L.; Zhu, Z. Ammonia-induced robust photocatalytic hydrogen evolution of graphitic carbon nitride. *Nanoscale* **2015**, *7*, 18887–18890.
53. Papailias, I.; Todorova, N.; Giannakopoulou, T.; Ioannidis, N.; Dallas, P.; Dimotikali, D.; Trapalis, C. Novel torus shaped g-C_3N_4 photocatalysts. *Appl. Catal. B Environ.* **2020**, *268*, 118733.
54. Li, H.J.; Sun, B.W.; Sui, L.; Qian, D.J.; Chen, M. Preparation of water-dispersible porous g-C_3N_4 with improved photocatalytic activity by chemical oxidation. *Phys. Chem. Chem. Phys.* **2015**, *17*, 3309–3315.
55. Shi, L.; Chang, K.; Zhang, H.; Hai, X.; Yang, L.; Wang, T.; Ye, J. Drastic Enhancement of Photocatalytic Activities over Phosphoric Acid Protonated Porous g-C_3N_4 Nanosheets under Visible Light. *Small* **2016**, *12*, 4431–4439.
56. Niu, P.; Zhang, L.; Liu, G.; Cheng, H.-M. Graphene-Like Carbon Nitride Nanosheets for Improved Photocatalytic Activities. *Adv. Funct. Mater.* **2012**, *22*, 4763–4770.
57. Cui, L.; Liu, Y.; Fang, X.; Yin, C.; Li, S.; Sun, D.; Kang, S. Scalable and clean exfoliation of graphitic carbon nitride in NaClO solution: Enriched surface active sites for enhanced photocatalytic H_2 evolution. *Green Chem.* **2018**, *20*, 1354–1361.
58. Babu, A. M.; Rajeev, R.; Thadathil, D. A.; Varghese, A.; Hegde, G. Surface modulation and structural engineering of graphitic carbon nitride for electrochemical sensing applications. *J. Nanostructure Chemistry* **2021**, *12*, 765–807.
59. Qi, K.; Liu, S.-y.; Zada, A. Graphitic carbon nitride, a polymer photocatalyst. *J. Taiwan Inst. Chem. Eng.* **2020**, *109*, 111–

123.
60. Umapathi, R.; Venkateswara Raju, C.; Majid Ghoreishian, S.; Mohana Rani, G.; Kumar, K.; Oh, M.-H.; Pil Park, J.; Suk Huh, Y. Recent advances in the use of graphitic carbon nitride-based composites for the electrochemical detection of hazardous contaminants. *Coordin. Chem. Rev.* **2022**, *470*, 214708.
61. Yang, B.; Han, J.; Zhang, Q.; Liao, G.; Cheng, W.; Ge, G.; Liu, J.; Yang, X.; Wang, R.; Jia, X. Carbon defective g-C_3N_4 thin-wall tubes for drastic improvement of photocatalytic H_2 production. *Carbon* **2023**, *202*, 348–357.
62. Li, C.; Jia, R.; Yang, Y.; Liao, G. A Hierarchical Helical Carbon Nanotube Fiber Artificial Ligament. *Adv. Fiber Mater.* **2023,** *5*, 1549-1551.
63. Liu, J.; Song, Y.; Xu, H.; Zhu, X.; Lian, J.; Xu, Y.; Zhao, Y.; Huang, L.; Ji, H.; Li, H. Non-metal photocatalyst nitrogen-doped carbon nanotubes modified mpg-C(3)N(4):facile synthesis and the enhanced visible-light photocatalytic activity. *J. Colloid Interface Sci.* **2017**, *494*, 38–46.
64. Wu, M.; Zhang, J.; He, B.-b.; Wang, H.-w.; Wang, R.; Gong, Y.-s. In-situ construction of coral-like porous P-doped g-C_3N_4 tubes with hybrid 1D/2D architecture and high efficient photocatalytic hydrogen evolution. *Appl. Catal. B Environ.* **2019**, *241*, 159–166.
65. Liao, G.; Zhang, L.; Li, C.; Liu, S.-Y.; Fang, B.; Yang, H. Emerging carbon-supported single-atom catalysts for biomedical applications. *Matter* **2022,** *5*, 3341-3374.
66. Han, Q.; Chen, N.; Zhang, J.; Qu, L. Graphene/graphitic carbon nitride hybrids for catalysis. *Mater. Horiz.* **2017**, *4*, 832–850.
67. Ji, H.; Du, P.; Zhao, D.; Li, S.; Sun, F.; Duin, E.C.; Liu, W. 2D/1D graphitic carbon nitride/titanate nanotubes heterostructure for efficient photocatalysis of sulfamethazine under solar light: Catalytic "hot spots" at the rutile–anatase–titanate interfaces. *Appl. Catal. B Environ.* **2020**, *263*, 118357.
68. Wen, J.; Wang, Y.; Zhao, H.; Zhang, M.; Zhang, S.; Liu, Y.; Zhai, Y. Uracil-mediated supramolecular assembly for C-enriched porous carbon nitrides with enhanced photocatalytic hydrogen evolution. *New J. Chem.* **2022**, *46*, 4647–4653.
69. Bu, L.; Xie, Q.; Ming, H. Gold nanoparticles decorated three-dimensional porous graphitic carbon nitrides for sensitive anodic stripping voltammetric analysis of trace arsenic(III). *J. Alloys Compounds* **2020**, *823*, 153723.
70. Wang, C.; Liu, G.; Song, K.; Wang, X.; Wang, H.; Zhao, N.; He, F. Three-Dimensional Hierarchical Porous Carbon/Graphitic Carbon Nitride Composites for Efficient Photocatalytic Hydrogen Production. *ChemCatChem* **2019**, *11*, 6364–6371.
71. Chen, X.; Shi, R.; Chen, Q.; Zhang, Z.; Jiang, W.; Zhu, Y.; Zhang, T. Three-dimensional porous g-C_3N_4 for highly efficient photocatalytic overall water splitting. *Nano Energy* **2019**, *59*, 644–650.
72. Di, J.; Xia, J.; Li, X.; Ji, M.; Xu, H.; Chen, Z.; Li, H. Constructing confined surface carbon defects in ultrathin graphitic carbon nitride for photocatalytic free radical manipulation. *Carbon* **2016**, *107*, 1–10.
73. Niu, P.; Qiao, M.; Li, Y.; Huang, L.; Zhai, T. Distinctive defects engineering in graphitic carbon nitride for greatly extended visible light photocatalytic hydrogen evolution. *Nano Energy* **2018**, *44*, 73–81.
74. Li, Y.; He, Z.; Liu, L.; Jiang, Y.; Ong, W.-J.; Duan, Y.; Ho, W.; Dong, F. Inside-and-out modification of graphitic carbon nitride (g-C_3N_4) photocatalysts via defect engineering for energy and environmental science. *Nano Energy* **2023**, *105*, 108032.
75. Yang, Q.; Yang, W.; He, F.; Liu, K.; Cao, H.; Yan, H. One-step synthesis of nitrogen-defective graphitic carbon nitride for improving photocatalytic hydrogen evolution. *J. Hazard. Mater.* **2021**, *410*, 124594.
76. Shcherban, N.D.; Filonenko, S.M.; Ovcharov, M.L.; Mishura, A.M.; Skoryk, M.A.; Aho, A.; Murzin, D.Y. Simple method for preparing of sulfur–doped graphitic carbon nitride with superior activity in CO_2 photoreduction, *ChemistrySelect* **2016**, *1*, 4987–4993.
77. Yang, B.; Li, X.; Zhang, Q.; Yang, X.; Wan, J.; Liao, G.; Zhao, J.; Wang, R.; Liu, J.; Rodriguez, R. D.; et al. Ultrathin porous carbon nitride nanosheets with well-tuned band structures via carbon vacancies and oxygen doping for significantly boosting H_2 production. *Appl. Catal. B Environ.* **2022**, *314*, 121521.
78. Qi, K.; Cui, N.; Zhang, M.; Ma, Y.; Wang, G.; Zhao, Z.; Khataee, A. Ionic liquid-assisted synthesis of porous boron-doped graphitic carbon nitride for photocatalytic hydrogen production. *Chemosphere* **2021**, *272*, 129953.
79. Yang, B.; Wang, Z.; Zhao, J.; Sun, X.; Wang, R.; Liao, G.; Jia, X. 1D/2D carbon-doped nanowire/ultra-thin nanosheet g-C_3N_4 isotype heterojunction for effective and durable photocatalytic H_2 evolution. *Int. J. Hydrogen Energy* **2021**, *46*, 25436–25447.
80. Feng, L.-L.; Zou, Y.; Li, C.; Gao, S.; Zhou, L.-J.; Sun, Q.; Fan, M.; Wang, H.; Wang, D.; Li, G.-D.; et al. Nanoporous sulfur-doped graphitic carbon nitride microrods: A durable catalyst for visible-light-driven H_2 evolution. *Int. J. Hydrogen Energy* **2014**, *39*, 15373–15379.
81. Kesavan, G.; Vinothkumar, V.; Chen, S.-M.; Thangadurai, T.D. Construction of metal-free oxygen-doped graphitic carbon nitride as an electrochemical sensing platform for determination of antimicrobial drug metronidazole. *Appl. Surf. Sci.* **2021**, *556*, 149814.
82. Wang, X.; Liu, B.; Xiao, X.; Wang, S.; Huang, W. Boron dopant simultaneously achieving nanostructure control and electronic structure tuning of graphitic carbon nitride with enhanced photocatalytic activity. *J. Mater. Chem. C* **2021**, *9*, 14876–14884.
83. Long, X.; Feng, C.; Yang, S.; Ding, D.; Feng, J.; Liu, M.; Chen, Y.; Tan, J.; Peng, X.; Shi, J.; et al. Oxygen doped graphitic carbon nitride with regulatable local electron density and band structure for improved photocatalytic degradation of

bisphenol A. *Chem. Eng. J.* **2022**, *435*, 134835.
84. Liu, B.; Ye, L.; Wang, R.; Yang, J.; Zhang, Y.; Guan, R.; Tian, L.; Chen, X. Phosphorus-Doped Graphitic Carbon Nitride Nanotubes with Amino-rich Surface for Efficient CO(2) Capture, Enhanced Photocatalytic Activity, and Product Selectivity. *ACS Appl. Mater. Interfaces* **2018**, *10*, 4001–4009.
85. Reddy, I. N.; Reddy, L.V.; Jayashree, N.; Reddy, C.V.; Cho, M.; Kim, D.; Shim, J. Vanadium-doped graphitic carbon nitride for multifunctional applications: Photoelectrochemical water splitting and antibacterial activities. *Chemosphere* **2021**, *264*, 128593.
86. Viet, N.M.; Trung, D.Q.; Giang, B.L.; Tri, N.L.M.; Thao, P.; Pham, T.H.; Kamand, F.Z.; Al Tahtamouni, T.M. Noble metal -doped graphitic carbon nitride photocatalyst for enhancement photocatalytic decomposition of antibiotic pollutant in wastewater under visible light. *J. Water Process Eng.* **2019**, *32*, 100954.
87. Yan, Y.; Yang, Q.; Shang, Q.; Ai, J.; Yang, X.; Wang, D.; Liao, G. Ru doped graphitic carbon nitride mediated peroxymonosulfate activation for diclofenac degradation via singlet oxygen. *Chem. Eng. J.* **2022**, *430*, 133174.
88. Yang, M.; Wang, K.; Li, Y.; Yang, K.; Jin, Z. Pristine hexagonal CdS assembled with NiV LDH nanosheet formed p-n heterojunction for efficient photocatalytic hydrogen evolution. *Appl. Surf. Sci.* **2021**, *548*, 149212.
89. Zhang, Y.; Sun, A.; Xiong, M.; Macharia, D. K.; Liu, J.; Chen, Z.; Li, M.; Zhang, L. TiO_2/BiOI p-n junction-decorated carbon fibers as weavable photocatalyst with UV–vis photoresponsive for efficiently degrading various pollutants. *Chem. Eng. J.* **2021**, *415*, 129019.
90. Guo, X.; Peng, Y.; Liu, G.; Xie, G.; Guo, Y.; Zhang, Y.; Yu, J. An Efficient $ZnIn_2S_4$@$CuInS_2$ Core–Shell p–n Heterojunction to Boost Visible-Light Photocatalytic Hydrogen Evolution. *J. Phys. Chem. C* **2020**, *124*, 5934–5943.
91. Tian, F.; Wu, X.; Liu, S.; Gu, Y.; Lin, Z.; Zhang, H.; Yan, X.; Liao, G. Boosting photocatalytic H_2 evolution through interfacial manipulation on a lotus seedpod shaped Cu_2O/g-C_3N_4 p-n heterojunction. *Sustainable Energy Fuels* **2023**, *7*, 786–796.
92. Zhang, Y.-J.; Cheng, J.-Z.; Xing, Y.-Q.; Tan, Z.-R.; Liao, G.; Liu, S.-Y. Solvent-exfoliated D-A π-polymer @ ZnS heterojunction for efficient photocatalytic hydrogen evolution. *Mater. Sci. Semiconductor Processing* **2023**, *161*, 107463.
93. Paramanik, L.; Reddy, K. H.; Parida, K. M. An energy band compactable B-rGO/PbTiO(3) p-n junction: A highly dynamic and durable photocatalyst for enhanced photocatalytic H(2) evolution. *Nanoscale* **2019**, *11*, 22328–22342.
94. Hao, R.; Wang, G.; Jiang, C.; Tang, H.; Xu, Q. In situ hydrothermal synthesis of g-C_3N_4/TiO_2 heterojunction photocatalysts with high specific surface area for Rhodamine B degradation. *Appl. Surf. Sci.* **2017**, *411*, 400–410.
95. Li, C.; Lu, H.; Ding, G.; Li, Q.; Liao, G. Recent advances on g-C_3N_4-based Z-scheme photocatalysts for organic pollutant removal. *Catal. Sci. Technol.* **2023**, *13*, 2877–2898.
96. Liao, G.; Li, C.; Liu, S.-Y.; Fang, B.; Yang, H. Z-scheme systems: From fundamental principles to characterization, synthesis, and photocatalytic fuel-conversion applications. *Phys. Rep.* **2022**, *983*, 1–41.
97. Zhu, H.; Zhang, C.; Xie, K.; Li, X.; Liao, G. Photocatalytic degradation of organic pollutants over MoS_2/Ag-$ZnFe_2O_4$ Z-scheme heterojunction: Revealing the synergistic effects of exposed crystal facets, defect engineering, and Z-scheme mechanism. *Chem. Eng. J.* **2023**, *453*, 139775.
98. Liao, G.; Li, C.; Liu, S.-Y.; Fang, B.; Yang, H. Emerging frontiers of Z-scheme photocatalytic systems. *Trends Chem.* **2022**, *4*, 111–127.
99. Liao, G.; Li, C.; Li, X.; Fang, B. Emerging polymeric carbon nitride Z-scheme systems for photocatalysis. *Cell Rep. Phys. Sci.* **2021**, *2*, 100355.
100. Chouchene, B.; Gries, T.; Balan, L.; Medjahdi, G.; Schneider, R. Graphitic carbon nitride/SmFeO(3) composite Z-scheme photocatalyst with high visible light activity. *Nanotechnology* **2020**, *31*, 465704.
101. Aminov, R. I. A brief history of the antibiotic era: Lessons learned and challenges for the future. *Front. Microbiol.* **2010**, *1*, 134.
102. Ardal, C.; Balasegaram, M.; Laxminarayan, R.; McAdams, D.; Outterson, K.; Rex, J. H.; Sumpradit, N. Antibiotic development-economic, regulatory and societal challenges. *Nat. Rev. Microbiol.* **2020**, *18*, 267–274.
103. D'Costa, V. M.; McGrann, K. M.; Hughes, D. W.; Wright, G. D. Sampling the antibiotic resistome. *Science* **2006**, *311*, 374–377.
104. Chang, Q.; Ali, A.; Su, J.; Wen, Q.; Bai, Y.; Gao, Z. Simultaneous removal of nitrate, manganese, and tetracycline by Zoogloea sp. MFQ7: Adsorption mechanism of tetracycline by biological precipitation. *Bioresour. Technol.* **2021**, *340*, 125690.
105. Gopal, G.; Alex, S. A.; Chandrasekaran, N.; Mukherjee, A. A review on tetracycline removal from aqueous systems by advanced treatment techniques. *RSC Adv.* **2020**, *10*, 27081–27095.
106. He, Z.; Wang, X.; Luo, Y.; Zhu, Y.; Lai, X.; Shang, J.; Chen, J.; Liao, Q. Effects of suspended particulate matter from natural lakes in conjunction with coagulation to tetracycline removal from water. *Chemosphere* **2021**, *277*, 130327.
107. Ortiz-Ramos, U.; Leyva-Ramos, R.; Mendoza-Mendoza, E.; Aragón-Piña, A. Removal of tetracycline from aqueous solutions by adsorption on raw Ca-bentonite. Effect of operating conditions and adsorption mechanism. *Chem. Eng. J.* **2022**, *432*, 134428.
108. Zhou, J.; Ma, F.; Guo, H.; Su, D. Activate hydrogen peroxide for efficient tetracycline degradation via a facile assembled carbon-based composite: Synergism of powdered activated carbon and ferroferric oxide nanocatalyst. *Appl. Catal. B: Environ.* **2020**, *269*, 118784.
109. Zhang, Q.; Jiang, L.; Wang, J.; Zhu, Y.; Pu, Y.; Dai, W. Photocatalytic degradation of tetracycline antibiotics using three-

dimensional network structure perylene diimide supramolecular organic photocatalyst under visible-light irradiation. *Appl. Catal. B Environ.* **2020**, *277*, 119122.
110. Duan, M.; Jiang, L.; Shao, B.; Feng, C.; Yu, H.; Guo, H.; Chen, H.; Tang, W. Enhanced visible-light photocatalytic degradation activity of Ti_3C_2/PDIsm via π–π interaction and interfacial charge separation: Experimental and theoretical investigations. *Appl. Catal. B Environ.* **2021**, *297*, 120439.
111. Dai, Y.; Liu, M.; Li, J.; Yang, S.; Sun, Y.; Sun, Q.; Wang, W.; Lu, L.; Zhang, K.; Xu, J.; et al. A review on pollution situation and treatment methods of tetracycline in groundwater. *Sep. Sci. Technol.* **2019**, *55*, 1005–1021.
112. He, X.; Kai, T.; Ding, P. Heterojunction photocatalysts for degradation of the tetracycline antibiotic: A review. *Environ. Chem. Lett.* **2021**, *19*, 4563–4601.
113. Marshall, B. M.; Levy, S. B. Food animals and antimicrobials: Impacts on human health. *Clin. Microbiol. Rev.* **2011**, *24*, 718–733.
114. Panneri, S.; Ganguly, P.; Nair, B. N.; Mohamed, A. A.; Warrier, K. G.; Hareesh, U. N. Role of precursors on the photophysical properties of carbon nitride and its application for antibiotic degradation. *Environ. Sci. Pollut. Res. Int.* **2017**, *24*, 8609–8618.
115. Hong, J.; Hwang, D.K.; Selvaraj, R.; Kim, Y. Facile synthesis of Br-doped g-C_3N_4 nanosheets via one-step exfoliation using ammonium bromide for photodegradation of oxytetracycline antibiotics. *J. Ind. Eng. Chem.* **2019**, *79*, 473–481.
116. Bao, J.; Bai, W.; Wu, M.; Gong, W.; Yu, Y.; Zheng, K.; Liu, L. Template-mediated copper doped porous g-C(3)N(4) for efficient photodegradation of antibiotic contaminants. *Chemosphere* **2022**, *293*, 133607.
117. Zhou, T.; Li, T.; Hou, J.; Wang, Y.; Hu, B.; Sun, D.; Wu, Y.; Jiang, W.; Che, G.; Liu, C. Tailoring boron doped intramolecular donor–acceptor integrated carbon nitride skeleton with propelling photocatalytic activity and mechanism insight. *Chem. Eng. J.* **2022**, *445*, 136643.
118. Zhang, Y.; Yuan, J.; Ding, Y.; Zhang, B.; Zhang, S.; Liu, B. Metal-free N-GQDs/P-g-C_3N_4 photocatalyst with broad-spectrum response: Enhanced exciton dissociation and charge migration for promoting H_2 evolution and tetracycline degradation. *Sep. Purif. Technol.* **2023**, *304*, 122297.
119. Thi Quyen, V.; Jae Kim, H.; Kim, J.; Thi Thu Ha, L.; Thi Huong, P.; My Thanh, D.; Minh Viet, N.; Quang Thang, P. Synthesizing S-doped graphitic carbon nitride for improvement photodegradation of tetracycline under solar light. *Solar Energy* **2021**, *214*, 288–293.
120. Zhang, H.; Zeng, Y.; Wang, X.; Zhan, X.; Xu, J.; Jin, A.; Hong, B. Sea-Urchin carbon nitride with carbon vacancies (C-v) and oxygen substitution (O-s) for photodegradation of Tetracycline: Performance, mechanism insight and pathways. *Chem. Eng. J.* **2022**, *446*, 137053.
121. Preeyanghaa, M.; Vinesh, V.; Neppolian, B. Complete removal of Tetracycline by sonophotocatalysis using ultrasound-assisted hierarchical graphitic carbon nitride nanorods with carbon vacancies. *Chemosphere* **2022**, *287*, 132379.
122. Ghosh, U.; Majumdar, A.; Pal, A. 3D macroporous architecture of self-assembled defect-engineered ultrathin g-C3N4 nanosheets for tetracycline degradation under LED light irradiation. *Mater. Res. Bull.* **2021**, *133*, 111074.
123. Jiang, D.; Ma, W.; Xiao, P.; Shao, L.; Li, D.; Chen, M. Enhanced photocatalytic activity of graphitic carbon nitride/carbon nanotube/Bi(2)WO(6) ternary Z-scheme heterojunction with carbon nanotube as efficient electron mediator. *J. Colloid Interface Sci.* **2018**, *512*, 693–700.
124. Jingyu, H.; Ran, Y.; Zhaohui, L.; Yuanqiang, S.; Lingbo, Q.; Nti Kani, A. In-situ growth of ZnO globular on g-C_3N_4 to fabrication binary heterojunctions and their photocatalytic degradation activity on tetracyclines. *Solid State Sci.* **2019**, *92*, 60–67.
125. Wang, H.; Zhao, Y.; Zhan, X.; Yu, J.; Chen, L.; Sun, Y.; Shi, H. Calcination synthesis of tin niobate loaded porous carbon nitride S-scheme heterojunction for photocatalytic H_2 production and tetracycline degradation. *J. Alloys Compounds* **2022**, *899*, 163250.
126. Mateen, M.; Cheong, W.-C.; Zheng, C.; Talib, S. H.; Zhang, J.; Zhang, X.; Liu, S.; Chen, C.; Li, Y. Molybdenum atomic sites embedded 1D carbon nitride nanotubes as highly efficient bifunctional photocatalyst for tetracycline degradation and hydrogen evolution. *Chem. Eng. J.* **2023**, *451*, 138305.
127. Chen, M.; Chu, W. Photocatalytic degradation and decomposition mechanism of fluoroquinolones norfloxacin over bismuth tungstate: Experiment and mathematic model. *Appl. Catal. B Environ.* **2015**, *168–169*, 175–182.
128. Yang, S.; Xu, D.; Chen, B.; Luo, B.; Shi, W. In-situ synthesis of a plasmonic Ag/AgCl/Ag_2O heterostructures for degradation of ciprofloxacin. *Appl. Catal. B Environ.* **2017**, *204*, 602–610.
129. Guo, F.; Zhang, H.; Li, H.; Shen, Z. Modulating the oxidative active species by regulating the valence of palladium cocatalyst in photocatalytic degradation of ciprofloxacin. *Appl. Catal. B Environ.* **2022**, *306*, 121092.
130. Van Doorslaer, X.; Demeestere, K.; Heynderickx, P. M.; Van Langenhove, H.; Dewulf, J. UV-A and UV-C induced photolytic and photocatalytic degradation of aqueous ciprofloxacin and moxifloxacin: Reaction kinetics and role of adsorption. *Appl. Catal. B Environ.* **2011**, *101*, 540–547.
131. Zhao, R.; Wang, Y.; An, Y.; Yang, L.; Sun, Q.; Ma, J.; Zheng, H. Chitin-biocalcium as a novel superior composite for ciprofloxacin removal: Synergism of adsorption and flocculation. *J. Hazard. Mater.* **2022**, *423*, 126917.
132. Alonso, J. J. S.; El Kori, N.; Melian-Martel, N.; Del Rio-Gamero, B. Removal of ciprofloxacin from seawater by reverse osmosis. *J. Environ. Manage* **2018**, *217*, 337–345.
133. Chuaicham, C.; Sekar, K.; Xiong, Y.; Balakumar, V.; Mittraphab, Y.; Shimizu, K.; Ohtani, B.; Dabo, I.; Sasaki, K. Single-step synthesis of oxygen-doped hollow porous graphitic carbon nitride for photocatalytic ciprofloxacin decomposition.

Chem. Eng. J. **2021**, *425*, 130502.
134. Balakumar, V.; Ramalingam, M.; Sekar, K.; Chuaicham, C.; Sasaki, K. Fabrication and characterization of carbon quantum dots decorated hollow porous graphitic carbon nitride through polyaniline for photocatalysis. *Chem. Eng. J.* **2021**, *426*, 131739.
135. Wang, Y.; Li, X.; Lei, W.; Zhu, B.; Yang, J. Novel carbon quantum dot modified g-C_3N_4 nanotubes on carbon cloth for efficient degradation of ciprofloxacin. *Appl. Surf. Sci.* **2021**, *559*, 149967.
136. Li, R.; Chen, A.; Deng, Q.; Zhong, Y.; Kong, L.; Yang, R. Well-designed MXene-derived Carbon-doped TiO_2 coupled porous g-C_3N_4 to enhance the degradation of ciprofloxacin hydrochloride under visible light irradiation. *Sep. Purif. Technol.* **2022**, *295*, 121254.
137. Qin, Y.; Yang, S.; You, X.; Liu, Y.; Qin, L.; Li, Y.; Zhang, W.; Liang, W. Carbon nitride coupled with Fe-based MOFs as an efficient photoelectrocatalyst for boosted degradation of ciprofloxacin: Mechanism, pathway and fate. *Sep. Purif. Technol.* **2022**, *296*, 121325.
138. Yang, Y.; Jin, H.; Zhang, C.; Gan, H.; Yi, F.; Wang, H. Nitrogen-deficient modified P–Cl co-doped graphitic carbon nitride with enhanced photocatalytic performance. *J. Alloys Compounds* **2020**, *821*, 153439.
139. Ding, D.; Yang, S.; Chen, L.; Cai, T. Degradation of norfloxacin by CoFe alloy nanoparticles encapsulated in nitrogen doped graphitic carbon (CoFe@N-GC) activated peroxymonosulfate. *Chem. Eng. J.* **2020**, *392*, 123725.
140. Li, C.; Sun, T.; Yi, G.; Zhang, D.; Zhang, Y.; Lin, X.; Liu, J.; Shi, Z.; Lin, Q. Microwave-assisted method synthesis of Ag/CNQDs/g-C_3N_4 with excellent photocatalytic activity for the degradation of norfloxacin. *Colloids Surfaces A Physicochem. Eng. Aspects* **2023**, *662*, 131001.
141. Van Thuan, D.; Nguyen, T.L.; Pham Thi, H.H.; Thanh, N.T.; Ghotekar, S.; Sharma, A.K.; Binh, M.T.; Nga, T.T.; Pham, T.-D.; Cam, D.P. Development of Indium vanadate and Silver deposited on graphitic carbon nitride ternary heterojunction for advanced photocatalytic degradation of residual antibiotics in aqueous environment. *Optical Mater.* **2022**, *123*, 111885.
142. Xiao, Y.; Lyu, H.; Yang, C.; Zhao, B.; Wang, L.; Tang, J. Graphitic carbon nitride/biochar composite synthesized by a facile ball-milling method for the adsorption and photocatalytic degradation of enrofloxacin. *J. Environ. Sci.* **2021**, *103*, 93–107.
143. Kumar, A.; Kumari, A.; Sharma, G.; Du, B.; Naushad, M.; Stadler, F. J. Carbon quantum dots and reduced graphene oxide modified self-assembled S@C_3N_4/B@C_3N_4 metal-free nano-photocatalyst for high performance degradation of chloramphenicol. *J. Mol. Liquids* **2020**, *300*, 112356.
144. Shojaeimehr, T.; Tasbihi, M.; Acharjya, A.; Thomas, A.; Schomäcker, R.; Schwarze, M. Impact of operating conditions for the continuous-flow degradation of diclofenac with immobilized carbon nitride photocatalysts. *J. Photochem. Photobiol. A Chem.* **2020**, *388*, 112182.
145. Zhong, J.; Ni, T.; Huang, J.; Li, D.; Tan, C.; Liu, Y.; Chen, P.; Wen, C.; Liu, H.; Wang, Z.; et al. Directional utilization disorder charge via In-plane driving force of functionalized graphite carbon nitride for the robust photocatalytic degradation of fluoroquinolone. *Chem. Eng. J.* **2022**, *442*, 135943.
146. Li, X.; Li, K.; Du, J.; Pei, M.; Song, C.; Guo, X. Nitrogen-rich porous polymeric carbon nitride with enhanced photocatalytic activity for synergistic removal of organic and heavy metal pollutants. *Environ. Sci. Nano* **2022**, *9*, 2388–2401.
147. Ding, H.; Liu, Z.; Zhang, Q.; He, X.; Feng, Q.; Wang, D.; Ma, D. Biomass porous carbon as the active site to enhance photodegradation of oxytetracycline on mesoporous g-C(3)N(4). *RSC Adv.* **2022**, *12*, 1840–1849.
148. Chuaicham, C.; Sekar, K.; Balakumar, V.; Mittraphab, Y.; Shimizu, K.; Ohtani, B.; Sasaki, K. Fabrication of graphitic carbon nitride/ZnTi-mixed metal oxide heterostructure: Robust photocatalytic decomposition of ciprofloxacin. *J. Alloys Compounds* **2022**, *906*, 164294.
149. Liu, X.; Yang, Z.; Yang, Y.; Li, H. Carbon quantum dots sensitized 2D/2D carbon nitride nanosheets/bismuth tungstate for visible light photocatalytic degradation norfloxacin. *Chemosphere* **2022**, *287*, 132126.
150. Meng, Y.; Sun, J.; Guo, Y.; Chen, J.; Lou, Y. Two-dimensional polymerized carbon nitride coupled with (0 0 1)-facets-exposed titanium dioxide S-scheme heterojunction for photocatalytic degradation of norfloxacin. *Inorg. Chem. Commun.* **2022**, *142*, 109704.
151. Zhang, Y.; Chen, M.; Li, G.; Shi, C.; Wang, B.; Ling, Z. Exfoliated vermiculite nanosheets supporting tetraethylenepentamine for CO_2 capture. *Results Mater.* **2020**, *7*, 100102.